MARINE VERSUS NON-MARINE ENVIRONMENTS FOR THE JIBALAH GROUP, NW ARABIAN SHIELD: A SEDIMENTOLOGIC AND GEOCHEMICAL SURVEY AND REPORT OF POSSIBLE METAZOA IN THE DHAIQA FORMATION

Nathan Miller *

Environmental Research Center & Geological Sciences, University of Missouri at Rolla, Box 65409, Rolla, MO 65409, USA

Peter R. Johnson

JV Associates, 1242 Tenth Street NW, Washington DC 20001, USA

and Robert J. Stern

Geosciences Department, University of Texas at Dallas, Box 830688, Richardson, TX 75083-0688, USA

الخلاصة:

يتضمن تاريخ الدرع النوبي-العربي لعصر ما قبل الكامبري المتأخر إغلاق محيط موزمبيق،مع تصادم وتشكل التراكيب ذات الإتجاه الشمالي الجنوبي (نشأة نابيته – ٦٤٠–٦٨٠ مليون سنة)، ملحوقة بتمدد وقص ذو اتجاه شمال غرب ليشكل امتداد أحواض لنظام نصف خسيفة (نشأة نجد – أقل من ٦٤٠ مليون سنة). ملأت صخور حقبة الإديكارن المتنوعة لمجموعة الجبلة هذه الأحواض، متضمنة رواسب جيرية كثيفة في بيئات بحيرية وخليجية وبحرية ضحلة. وهناك خلاف حول تجمع رواسب مجموعة جبلة بالكامل فإما ترسبت في هذه الأحواض أو أنها ترسبت في تكوينات بحرية وحفظت محليا في هذه الأحواض. وتعتبر طبيعة ترسيب مجموعة جبلة ذات إهتمام مميز حيث أن الحقبة الإديكارينية تحتوى على أخر مراحل الكربوجينين الجليدية وأعظم مراحل التأريخ البحري للكربون السالب ($\delta^{13}C_{carb}$: شاذة شورم)، وأول ظهور للحيوانات متعددة الخلايا.

تم تقرير النتائج الترسيبية والجيوكيميائية لمتكون الضيقة، ذات الـ ٣٠٠ متر سماكة من التتابع الجيري لمجموعة جبلة والتي لم تدرس سابقا والواقعة في شمال غرب الدرع العربي من العصر الإديكاريني. حدث ترسيب متكون الضيقة بين ٦٠٠ إلي ٥٣٠ مليون سنة ضمن بيئة بحيرية أو خليجية أو بحرية غير مفصلة. يمكن تواجد أثر أحافير متعددة الخلايا في الجزء السفلي لمتكون الضيقة، أسفل معدن الزيركون الدايامكتيتي الحامل للفتات منذ ٥٩٩ مليون سنة (± ٤,٨ مليون سنة). وإذا ما تأكد، فلسوف يشير لوجود أثر الحيوانات المتعددة الخلايا لبيئة ترسيبية بحرية ولسياق بحري لتفسير أثار النظائر. تظهر مكونات نظير معدن السترونشيوم الواقعة بين ٠,٧٠٤–٠,٧٠٦ إلي تأثير دائم للسترونشيوم الإنسيماتيكي، والذي يمنع المضاهاة مع ماء بحر عصر الإديكارين. وإن المكونات النظائرية لعنصر الكربون والمقاومة لتغيرات ما بعد النشأة من خلال الموائع النيزيكية وتغيرات ما بعد الترسب هي موجبة وتتراوح ما بين +٢,٤ ± ٢,٣ %. إذا ما تم المحافظة على المكونات البحرية، ستساعد المكونات الموجبة على حصر نافذة ترسيب متكون الضيقة للفترة إما قبل (تقريبا ٦٠٠ مليون سنة إلي حوالي بعد عصر جازكيرز الجليدي، إحتمالا بين ٥٧٠–٥٦٠ مليون سنة) أو بعد (تقريبا ٥٥١ إلي ٥٤٢ مليون سنة) شاذة الشورم. المضاهاة السابقة منسجمة مع متكون خفي (مجموعة نافن) في سلطنة عمان أسفل تباين طباقي والذي ينسب لعصر الجازكيرز الجليدي، ولكن هذا يتضمن السجل القديم للشكل المعقد لأثر أحافير العصر الإديكاريني. المضاهاة الأخيرة منسجمة مع متكون بوه (مجموعة نافن) ومجموعة أرا وأقرب للوقت الذي تم فيه تمييز الجحور. يلزم عمل الكثير من الدراسات في الأحواض الجيرية لمجموعة جبلة لتقييم أي من هذه السيناريوهات الأكثر إحتمالية.

*Address for correspondence:
Department of Geological Science, University of Texas at Austin, Austin, TX 78712-0254
E-mail: nrmiller@mail.utexas.edu
Phone & Fax numbers: 512-471-4810 (O) 512-471-9425 (F)

Paper Received December 28, 2007; Accepted March 22, 2008

ABSTRACT

We report sedimentologic, geochemical, and zircon U-Pb geochronologic data for the Dhaiqa formation, a 300 m thick carbonate succession (Dhaiqa basin, NW Arabian shield) thought to represent one of Saudi Arabia's youngest Precambrian basement exposures within the Ediacaran age Jibalah Group. The evidence supports that Dhaiqa formation deposition occurred between ≤ 600 and ~530 Ma, within an unresolved lacustrine, paralic, or marine setting. Possible metazoan trace fossils occur in the lower part of the Dhaiqa formation, below a distinct diamictite interval that bears detrital zircons as young as 599 ± 4.8 (core) and 570 ± 4.6 (rim) Ma. If confirmed, the metazoan traces argue for a marine depositional setting and a marine context for interpreting isotopic signatures. Strontium isotope compositions between 0.704–0.706 demonstrate a prominent diagenetic and/or depositional influence by ensimatic Sr, which prohibits correlation with Ediacaran seawater. Carbon isotopic compositions, more resistant to diagenetic alteration by meteoric and diagenetic fluids, are predominantly positive, averaging +2.4 ± 2.3‰. If marine $\delta^{13}C_{carb}$ compositions are retained, the positive signatures constrain Dhaiqa formation deposition to the interval either before (~600 Ma to sometime after the Gaskiers glaciation, possibly 570–560 Ma) or after (~551 to 542 Ma) the Shuram anomaly–Earth's greatest marine negative $\delta^{13}C_{carb}$ excursion. The former correlation is consistent with the Khufai Formation (Nafun Group) in Oman below an unconformity attributed to the Gaskiers glaciation, but this implies the oldest record of behaviorally complex Ediacaran trace fossils. The latter correlation is consistent with the burrows recognized.

Key words: Arabian shield, Ediacaran, Gaskiers glaciation, chemostratigraphy, metazoa

MARINE VERSUS NON-MARINE ENVIRONMENTS FOR THE JIBALAH GROUP, NW ARABIAN SHIELD: A SEDIMENTOLOGIC AND GEOCHEMICAL SURVEY AND REPORT OF POSSIBLE METAZOA IN THE DHAIQA FORMATION

1. INTRODUCTION

This paper concerns the geologic context of Saudi Arabia's youngest Precambrian sediments as explored within the Dhaiqa formation (Jibalah Group), a spectacularly exposed Ediacaran age carbonate succession that is preserved within a small basin (Dhaiqa basin) in the northwestern Arabian shield (Figures (1) and (2)). The basin resides unconformably below the region's oldest Paleozoic sediments (Cambrian age Siq Sandstone – basal member of the Saq Sandstone) and provides a glimpse of Ediacaran sedimentation in the western Arabian shield. The discovery of possible metazoan fossils and glacial diamictite in the Dhaiqa succession has important implications for the Saudi Arabian Ediacaran record, if confirmed. Herein, we evaluate the lithostratigraphic character of the Dhaiqa formation, its age and place among regional Ediacaran depositional systems, and the extent to which it preserves a marine isotopic (C, O, Sr) record.

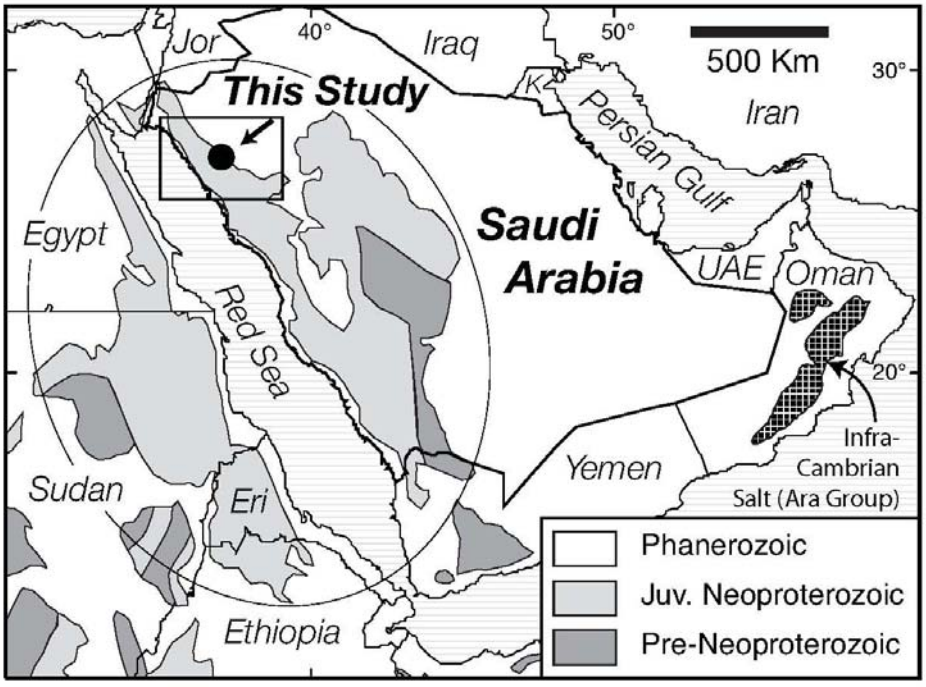

Figure 1. Location map of the Dhaiqa basin study area in the northwestern Arabian shield. The ellipse centered over the Red Sea indicates the distribution of juvenile Neoproterozoic crust that defines the Arabian–Nubian Shield. Oman infra-Cambrian (Neoproterozoic to Early Cambrian) salt basins bearing Nafun and Ara Group sediments possibly equivalent within the Jibalah Group of Saudi Arabia are shown by the square infill pattern (http://www.ged.rwth-aachen.de/Ww/projects/ogtech/saltdomes/saltdomes.html).

The Neoproterozoic segue to the first appearance of macroscopic heterotrophic life involved the Cryogenian (850–630 Ma) and Ediacaran (630–542 Ma) Periods (Figure 3). This dynamic interval of geologic time included the breakup of Rodinia and reassembly of Gondwana, repeated transitions to and from global icehouse climate states, and a major increase (or series of increases) in ocean–atmosphere oxygen content. Geologic investigations of how these episodes are manifest in global sedimentary records and how they may relate to metazoan radiation and diversity are the focus of vigorous international research–spurred on by the controversial Snowball Earth hypothesis and alternative models of Neoproterozoic climate change [1–3]. The number of glacial intervals and their respective durations and geographic extents are yet unresolved, and the temporal context of glacial interval terminology is evolving with the addition of high-resolution geochronologic data. Four late Neoproterozoic glacial intervals are presently recognized: (1) Kaigas (~750 Ma), (2) Sturtian (~711 to ~643 Ma); Marinoan (~635 Ma); and Gaskiers (~580 Ma) [4–3]. Of relevance to the present study is the uniquely Ediacaran Gaskiers glaciation. In contrast to earlier Cryogenian glaciations, the Gaskiers is widely considered to have been a lesser glaciation on the basis of limited geographic distribution, short duration on the order of

1 myrs, and lack of associated paleoceanographic phenomena (*e.g.*, a coincident negative $\delta^{13}C_{carb}$ excursion and occurrence of post-glacial cap carbonate). The appearance of Ediacaran fauna close to, or following, the Gaskiers glaciation, (575 Ma) demonstrates that a more oxygenated ocean–atmosphere system had emerged by this time [5,6].

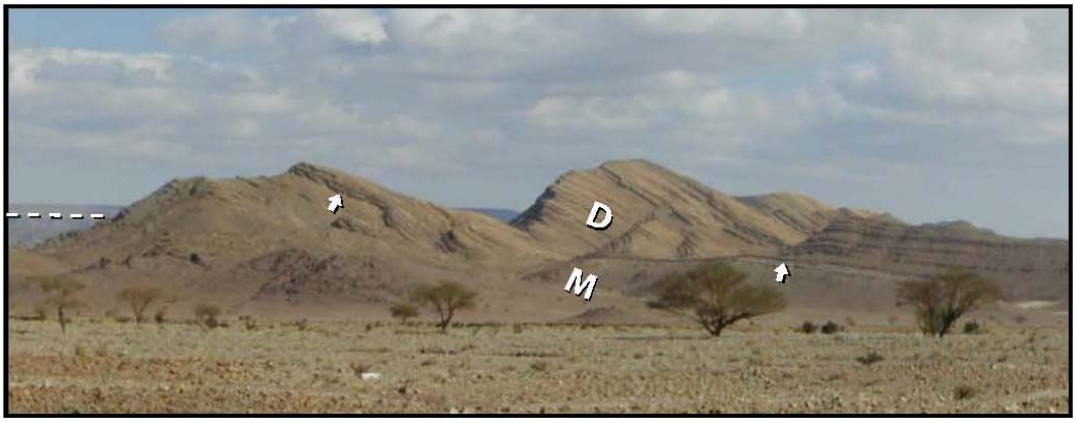

Figure 2. Northeastern view of the SSE-dipping Dhaiqa Ediacaran basin. The Dhaiqa formation (D) begins conformably above (arrows) the Mataar formation (M). The Dhaiqa formation transect begins at the top of the low ridge in the foreground (right arrow) and continues upsection to the right in the image. The Afro–Arabian peneplain (dashed line), separating Precambrian from Cambrian strata, occurs shortly below the horizon line at the left of the image.

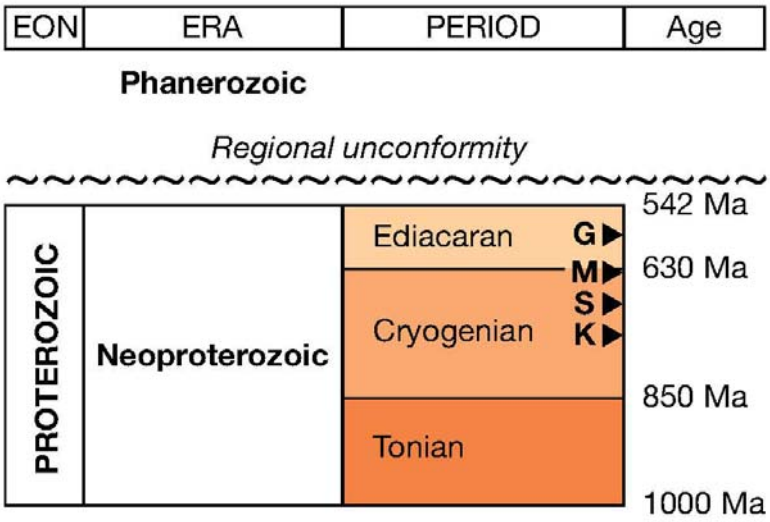

Figure 3. General chronostratigraphic framework of the northwestern Arabian shield area. Triangles denote the major Cryogenian glacial intervals: K = Kaigas, S = Sturtian, M = Marinoan, G = Gaskiers. Jibalah Group post-amalgamation basin sequences (including the Dhaiqa formation) preserve Saudi Arabia's youngest Ediacaran strata.

The Arabian–Nubian Shield (ANS) contains evidence of Cryogenian icehouse states [7]. Within the Arabian shield, prospective "Cryogenian" deposits include banded iron formation (Wadi Sawawin) and diamictite (Nuwaybah Formation) of probable "Sturtian" (or older) affiliation [7,8]. Evidence of Marinoan and Gaskiers glaciations has not been found, possibly because much of the region resided within the elevated setting of the East African Orogen (EAO) during this time [7]. Late Neoproterozoic erosion of this orogenic setting produced a widespread unconformity throughout North Africa and Arabia (here termed the Afro–Arabian Peneplain, or AAP) that separates Neoproterozoic from Lower Paleozoic strata [9]. The AAP is exceptionally well exposed throughout the western Arabian shield. Isolated Ediacaran sedimentary sections are known from Jibalah Group basins, indicating that the northern EAO was not entirely emergent during the Ediacaran Period. Further southeast in Oman, marine deposition spanning most of the Ediacaran Period is known [10]. There, sedimentological and geochemical evidence exists for the Sturtian and Marinoan glaciations, but no direct evidence has been found for the Gaskiers glaciation. Instead, only lithostratigraphic sequence boundaries have been linked to the Gaskiers [5].

Cryogenian and Ediacaran tectonic events in the Arabian shield involved closure of the Mozambique Ocean between fragments of W and E Gondwana, collision and deformation to form N-S trending structures (Nabitah orogeny; 680-640 Ma), followed by later NW-trending extension, and shearing (possibly related to extrusion tectonics) to form a system of half-graben transtensional basins (so–called Najd orogeny; <640 Ma). Lithologically diverse Ediacaran rocks of the Jibalah Group, including widespread carbonate sequences (some rich in organic matter with petroleum source rock potential), fill these basins. The "Najd" basins are typically small and disconnected within the Arabian shield (mainly north of 20°N) and subsurface of the Arabian Platform [11–13]. Because access to Jibalah Group outcrops is correspondingly limited, the Ediacaran sedimentary record of Saudi Arabia is poorly known.

Open marine isotopic records (C, O, Sr, S), as proxied by chemical sediments (chiefly well preserved carbonates), reveal the history of important Precambrian tectonic, chemical, and biological changes, and provide the basis for global chemostratigraphic correlation. It is debatable whether Jibalah basins originated as separate small fault basins or were formerly more extensive (or even regionally continuous with a shared stratigraphy) and are merely preserved in down-faulted structures [13]. As a result, the non-marine (paralic and/or lacustrine) versus marine origin of Jibalah Group carbonate successions is unclear. Given that the Ediacaran Period contains the last of the great Neoproterozoic glacial intervals, Earth's greatest marine negative $\delta^{13}C_{carb}$ excursion (the Shuram anomaly), and the first appearance of complex metazoans, well-preserved marine carbonate successions within the Jibalah Group could reveal much about Saudi Arabia's Ediacaran history.

2. GEOLOGIC SETTING

Dhaiqa Basin falls within a NW-trending zone of Ediacaran basins in the northwestern part of the Arabian shield (Figures 4 and 5). Davies *et al*. [14] and Davies [15] originally mapped the region and the units (Dhaiqa and Mataar formations) are so far only informally defined within the lithostratigraphic scheme of Saudi Arabia. The local basins (Dhaiqa, Dawqah, and Salih) discussed in this report are also informally named. These basins appear to be developed along segments of the Najd fault system–a system of mainly NW-trending sinistral strike slip faults that affected the Arabian shield toward the end of the Neoproterozoic. Some basins relate to Najd N-directed expulsion tectonics during the terminal collision of E and W Gondwana. The basins are commonly interpreted as pull apart basins, and their sedimentary records are assigned within the Jibalah Group. The Jibalah Group was originally defined in the central part of the Arabian shield [16], but has subsequently been mapped in the northwestern [17] and northeastern shield, and is also reported in drill holes from the Arabian Platform [13]. Further southeast, in Oman, deposition of the Nafun Group (*ca*. 635–547 Ma) was contemporaneous with the Jibalah Group [18].

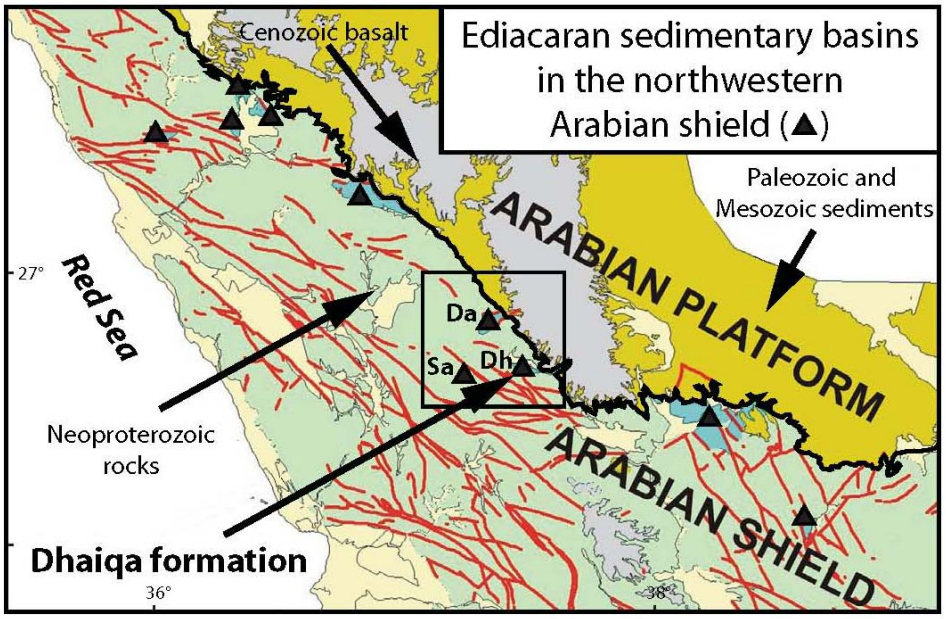

Figure 4. Regional geologic map of the northwestern Arabian shield showing the occurrence of isolated Ediacaran sedimentary basins (black triangles, blue map polygons) scattered below the Afro–Arabian Peneplain (cf. Figure 5). The bold black line delineates the main boundary between rocks of the shield and platform. Red lines show predominantly NW-trending (Najd system) faults. Square border shows three small Ediacaran basins - Dhaiqa (Dh), Dawqah (Da), and Salih (Sa) - within the general study area. Dhaiqa formation carbonate sediments are only found in Dhaiqa basin. Map is based on the 1:250 000 compilation of Davies [15] for the Al Wajh quadrangle.

Dhaiqa Basin is one of three small Ediacaran basins in the area (Figure 4, box), but the only one that is entirely sedimentary–involving conformable deposition of the Mataar (siliciclastic) and Dhaiqa (limestone) Formations (Figure 6). The other two basins (Salih and Dawqah, respectively to the W and NNW) contain siliciclastic and rhyolite flow sequences of the Misyal and Salih formations. Although the composite Mataar–Dhaiqa formational sequence tops the deformed Neoproterozoic sequence in this area, their respective age relations are unclear. Some possible Jibalah basins further to the NW are intruded by granite, which could be contemporaneous with basins containing rhyolite fill. However, other Jibalah basins predate the granite intrusions. The basins are grouped together under the term Jibalah considering their broadly contemporary (discussed below) volcanic and sedimentary successions in the NW, N, and NE shield.

Figure 5. Oblique topography-draped GoogleEarth™ satellite view of the Dhaiqa basin study area, showing the Dhaiqa formation transect route (white line) and sample localities (yellow squares, sample DY-1 shows the diamictite geochronology locality–see text), and proximity of the Arabian Platform and Afro-Arabian Peneplain (dashed line between Cambrian Saq Sandstone and Neoproterozoic strata). Vertical exaggeration is 300% (cf. Figure 4). Map units adopted from Davies [15]: gs = unassigned, but possibly Marabit affinity syenogranite (~620 Ma); bka = Bayda Group (<780->725) Ma; jm = Mataar formation. Eastward above its contact with the Mataar formation, the Dhaiqa formation is continuously exposed over a distance of 3 km.

Regional stratigraphic relationships and dated intrusives indicate a probable Ediacaran age for the Dhaiqa formation [15,20]. The oldest rocks in the area, both stratigraphically and tectonically, are deformed volcanic arc rocks of the Bayda Group. These were involved in 700–660 Ma arc amalgamation, along with the Zaam Group and coeval terranes in the NW Arabian shield [12]. A major sedimentary unit (Thalbah Group) was deposited between 660–620 Ma, unconformably on the Zaam and Bayda groups (SW of the study area). Marabit suite granites, having crystallization ages of 621 ± 7 Ma (Liban complex monzogranite, U–Pb model age on zircon [19], and 609 Ma (SHRIMP zircon ages from Hadb, Ash Shab, and Warid complex granitoids [20]), then intruded the region. The Mataar and Dhaiqa (together with Misyal and Salih) Formations are unconformable on 609 Ma granite complexes and the older deformed low-grade volcanic rocks [20]. Dhaiqa Basin is gently folded and down-faulted, indicating that the region was tectonically active after deposition of the Dhaiqa formation, although unlike older deformation events in the Arabian shield, deformation of the Dhaiqa was gentle and was not accompanied by any metamorphism or development of cleavage. Sometime after Dhaiqa deformation, near the end of the Precambrian, a profound low-relief erosional surface (part of the AAP) developed. The Siq Sandstone of probable Cambrian age (basal member of the Saq Sandstone) comprises the first sediments above the peneplain, and this contact is widely exposed throughout northwestern Arabia. Detrital zircon SHRIMP dating in Israel and Jordan (~390 km N of Dhaiqa basin) indicates a maximum age of 550–530 Ma for basal Cambrian sandstones equivalent to the lower part of the Saq Sandstone in Saudi Arabia, with the main concentration (650–550 Ma) consistent with Neoproterozoic detritus derived from the ANS [21,22]. The known geochronology

suggests that the conformable Mataar–Dhaiqa formation sequence in Dhaiqa Basin was deposited sometime between 609 and 530 Ma. Allowing time for development of the end-Precambrian peneplain, the maximum depositional age of the Dhaiqa formation is probably Ediacaran rather than Cambrian. More specific, local maximum and minimum age constraints remain to be determined.

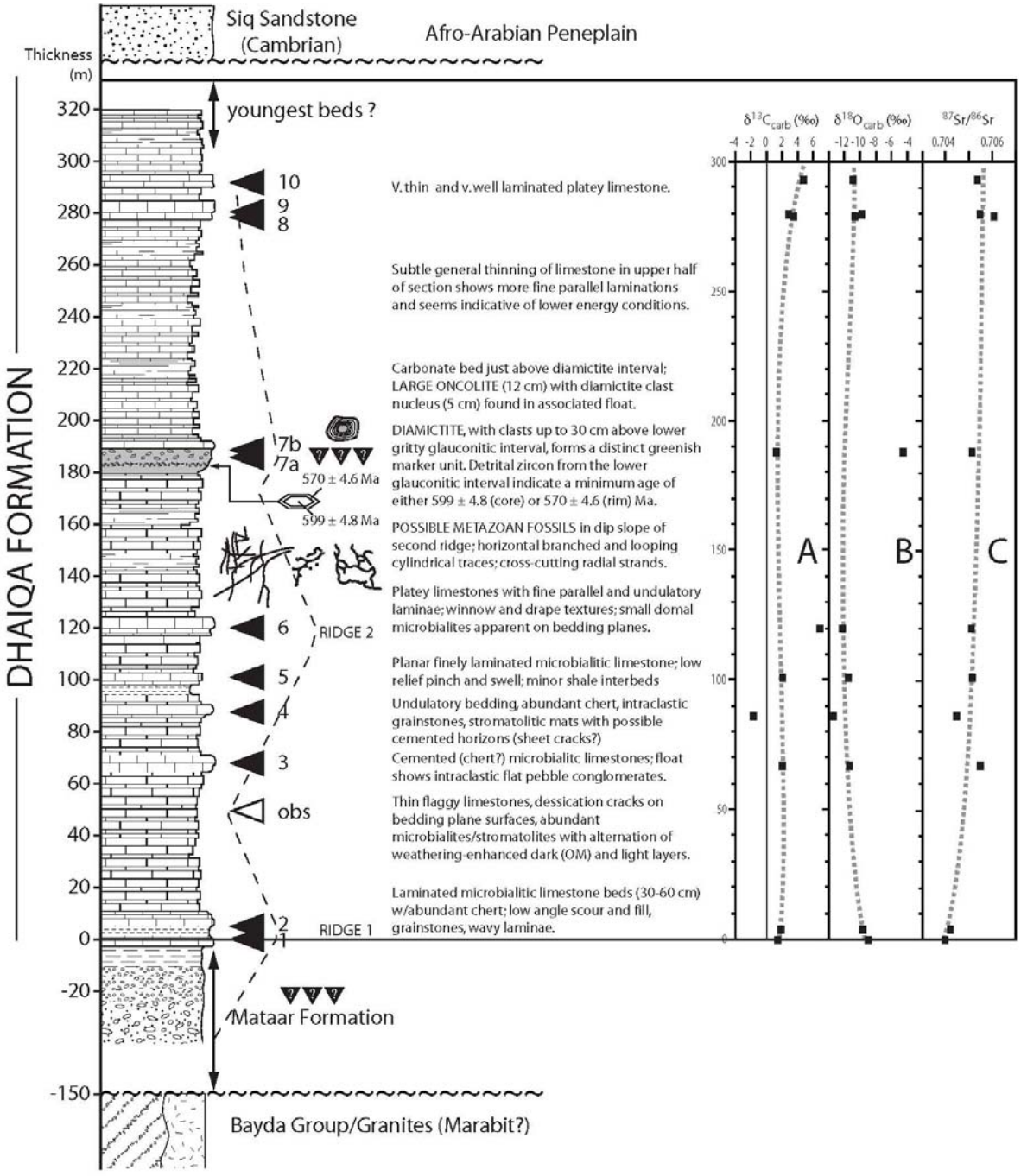

Figure 6. Stratigraphic column for the Dhaiqa formation transect, showing sampled horizons, significant sedimentologic observations, and corresponding $\delta^{13}C_{carb}$ and $\delta^{18}O_{carb}$ results (V-PDB). The dashed line to the right of the stratigraphic column shows the relative position of three ridges within the transect route. Polymict conglomerates (diamictites) occur in the Mataar formation and near 180 m in the Dhaiqa formation. Possible metazoan fossils occur above in the dip slope of the second ridge (above Sample 6).

We investigated the Dhaiqa formation type locality (Dhaiqa Basin) [14,15] west of Wadi Dhaiqa (centered near 22.6608N, 37.4373E, northwestern Al Madinah province). Here predominantly limestone beds of the Dhaiqa formation conformably overlie the Mataar formation (a polymictic conglomerate as much as 100 m thick) within an east-trending outcrop belt, roughly 3 km long by 0.5–1 km wide. Satellite imagery combined with field observations indicate that Dhaiqa basin is a broad open south-plunging syncline, which is elevated above the wadi plain along its northern and northwestern flanks (Figures 2, 5). The slightly curved dip slope exposes progressively younger Dhaiqa beds toward the interior of the structure. The steeper northern scarp flank exposes sub-horizontal strata of the Mataar and Dhaiqa formations above a steep angular unconformity with the underlying unit–possibly arkosic and conglomeratic strata of the upper Bayda Group [15]. Dips for the Mataar and Dhaiqa formations are moderate along the northern structural flank (>30–50° from photos), but decrease toward the younger interior of the syncline. Our east-trending sample transect, effectively through the west limb of the syncline, moved upsection in the dip direction, beginning in the upper part of the Mataar formation and ending in upper exposures of the Dhaiqa formation. The transect route intersected three ridges, each presenting a western scarp slope and an eastern dip slope (Figure 5). Dips are on the order of 18–20°.

3. METHODS

3.1. Sample Collection and Processing

In the field, GPS positions, photographs, and lithostratigraphic descriptions were recorded, and a representative rock sample taken, for each of 11 Dhaiqa formation localities. Bedding-normal thin sections (half-stained with Alizaren Red S and KFeCN) and mated polished rock slabs were prepared, and examined petrographically. Slab areas corresponding to thin section regions having well-preserved primary depositional textures (especially homogeneous micritic areas) were microdrilled to obtain 10–15 mg of powder, which was in turn split into aliquots for stable isotope and geochemical analyses. To lessen contamination by non-carbonate phases, powders for geochemistry were dissolved in volumes of weak acid (0.8M HOAc) sufficient to provide less than a two-fold molar excess above that required to dissolve the sample (assuming pure $CaCO_3$). The leachate was split into aliquots for ICP–OES (further diluted in 4% HNO_3) and Sr isotopes, and the dissolved carbonate (ASC) content determined from the insoluble residue.

3.2. ICP–OES

Major and minor cations (Ca, Mg, Fe, Mn, Sr) were determined on a Perkin–Elmer Optima 3300 DV inductively-coupled plasma optical emission spectrometry (ICP–OES) system in the Department of Geosciences at the University of Texas. Samples were measured using external calibration and results were checked for drift. Final solid concentrations were derived after adjusting for drift and all processing related dilutions.

3.3. Stable Isotopes

Powder splits were analyzed on a Finnigan-MAT 252 IRMA with a Kiel III automated carbonate device in the Paul H. Nelson Stable Isotope Laboratory at the University of Iowa. Approximately 0.05 to 0.10 mg of powder was reacted with 3 drops of anhydrous phosphoric acid at 75°C. Daily analysis of NIST powdered carbonate standards (NBS-18, 19, 20) and several in-house standards were conducted. Analytical precision on these standards was better than 0.1‰ for both $\delta^{18}O$ and $\delta^{13}C$ values. All results are reported in per mil (‰) relative to V-PDB.

3.4. $^{87}Sr/^{86}Sr$

Leachate strontium was extracted by standard procedures using Sr-specific resin (EIChromM Sr Resin SPS) and loaded onto rhenium filaments in a tantalum oxide and phosphoric acid slurry. Strontium isotopic compositions were determined using a Finnigan MAT-261 variable collector thermal ionization mass spectrometer at the University of Texas at Dallas. Samples were run in duplicate or triplicate. Isotopic measurement for each sample typically involved 100 static multicollection cycles of all four Sr isotopes in addition to ^{85}Rb, for monitoring ^{87}Rb. Mass discrimination during evaporation and ionization of Sr was corrected for by normalizing Sr isotopic ratios to $^{86}Sr/^{88}Sr = 0.1194$ using a linear correction scheme. During measurement, the $^{88}Sr^{+}$ ion beam was maintained at 3.5±0.5V on a $10^{-11}\Omega$ resistor. Strontium isotope standard NIST SRM-987 was measured prior to and following sample runs during each of three analytical sessions, and averaged 0.710270 ± 33 (n = 8). Precision for sample replicates was ± 22 ppm (n = 21). To facilitate comparison with other studies, $^{87}Sr/^{86}Sr$ results are normalized to a (more conventional) baseline of 0.710240.

3.5. Detrital Zircon Geochronology

For the purpose of geochronologic analysis, a ~2 kg sample (DY-1) was taken from a bed of fine-grained green sandstone within the sequence of limestone that forms the middle part of the Dhaiqa formation (comparable to sample 7a; fine-grained glaucarenite below polymict conglomerate in Figure 8B). The sample was prepared by MinSep

Laboratories, Western Australia, using conventional mineral separation techniques, after crushing and sieving, including a Wilfley table, heavy liquids, and the Frantz isodynamic separator. The final mineral separates consisted of handpicked, best-quality, non-magnetic grains, characterized by homogeneity, transparency, color, and fluorescence. Prior to SHRIMP analysis, zircon grains from the samples and a zircon standard were mounted and polished in a 24 mm diameter epoxy disc and gold coated. The zircons were then photographed and examined by cathodoluminescence (CL) imaging on a Philips X-30 SEM.

SHRIMP analyses were done on a SHRIMP RG2 instrument at the John de Laeter CEMS SHRIMP II, Curtin University, Perth, Western Australia, and details are reported in an Open-file report of the Saudi Geological Survey [20]. The instrumental techniques were similar to those of [23] and [25], and analyses were interspersed with the Curtin standard zircon crystal (CZ3). Off-line computer programs using standard techniques reduced all isotopic measurements. Pb/U ages were normalized to a value of 564 Ma determined by conventional U–Pb analysis of the standard zircon CZ3. The measurement of $^{206}Pb/^{238}U$ and $^{207}Pb/^{235}U$ ages requires normalization to the results of the standard analyses and the results were corrected for the uncertainties associated with the measurements of the CZ3 standard. Common-Pb was corrected for using the ^{204}Pb method discussed in [24] rather than the ^{208}Pb method [23]. Decay constants used are those recommended by the IUGS [25]. Data were collected during 5–7 cycles through nine magnetic-field values, and the resultant data set for all peaks over all cycles was used to calculate count rates integrated over time from the last peak of the first cycle to the first peak of the last cycle. These count rates were used to calculate isotopic ratios for the analysis.

Errors cited for individual analysis include errors from counting statistics, the common-Pb correction, and the U–Pb calibration error based on reproducibility of U–Pb measurements of the standard, and are at the 1σ level. Weighted mean values given on pooled analyses are at the 95% confidence level. Error boxes shown in Figure 11C are at the 1σ uncertainties.

4. RESULTS

4.1. Dhaiqa Formation Lithostratigraphy

Figure 6 shows the stratigraphic column and horizons sampled for the transect survey. Our estimate of ~300m for the Dhaiqa formation thickness is twice that of Davies *et al*. [14]. The basal section of our traverse begins in the upper part of the Mataar formation, exposed in the scarp face of the first ridge. The Mataar formation is a poorly bedded polymict conglomerate that grades upward into arkose and lithic arenite below the first carbonate beds of the Dhaiqa formation. Mataar conglomeratic clasts are poorly sorted, subangular to subrounded in shape, and vary in size; ranging up to m-scale outsized boulders (Figure 7A). Davies [15] described the unit as filling paleodepressions, and as having diverse clast lithologies, including rhyolite, dacite, andesite, monzogranite, and abundant alkalic granite. The nature of clast support (matrix *vs*. clast) was not obvious, but matrix support is indicated for the outsized boulders. The unit is consistent with molasse or fanglomerate, but matrix-supported outsized boulders also suggest a glacial diamictite. The Dhaiqa formation begins conformably above litharenite of the Mataar formation as intermittent limestone beds, followed by more-or-less continuous limestone deposition throughout the remainder of the unit (Figure 3). The Dhaiqa formation shows an overall stratigraphic progression from relatively energetic shallow water facies to lower energy facies in the upper portion of the unit. A 2–3 m thick diamictite interval near 180 m is a convenient marker bed that grossly separates these contrasting energy regimes (Figure 6).

The lower half of the Dhaiqa formation has abundant microbialite and peloidal grainstone facies, distinguished by undulatory laminated bedding that is enhanced by differential weathering. Lamination is generally thin (< 1mm) and ranges from parallel to irregular, the latter in association with calcite spar-filled cavities ("birdseye" structures). Grainstones commonly fill lows and thin over highs, with highs often corresponding to thicker (early gas filled or cemented?) microbialites (Figure 7B). Occurrence of desiccation cracks and intraclastic grainstones (edgewise conglomerates) suggest a shallow intertidal or supertidal environment above storm wavebase (Figure 7C–D). Stromatolitic biostromes exhibit abundant undulatory–stratiform cement horizons (Figure 7E) alternating with comparatively thinner layers (organic-rich algal mats). Many of the thicker resistant limestone ridges in the Dhaiqa formation may be well-cemented biostromes. Chert cementation as nodules and horizons is a common component of biostromes (Figure 7B, E). Microbialites are principally non-columnar mats, but low relief laterally linked hemispheroid morphologies are also preserved along bedding planes (Figure 7F). In bedding plane exposures, many microbialites reveal dark pustular regions of the underlying mat surface, probably representing a carbonaceous algal matter. The latter layers also form intraclasts, indicating that algal mats were likely prone to episodic delamination and fragmenting.

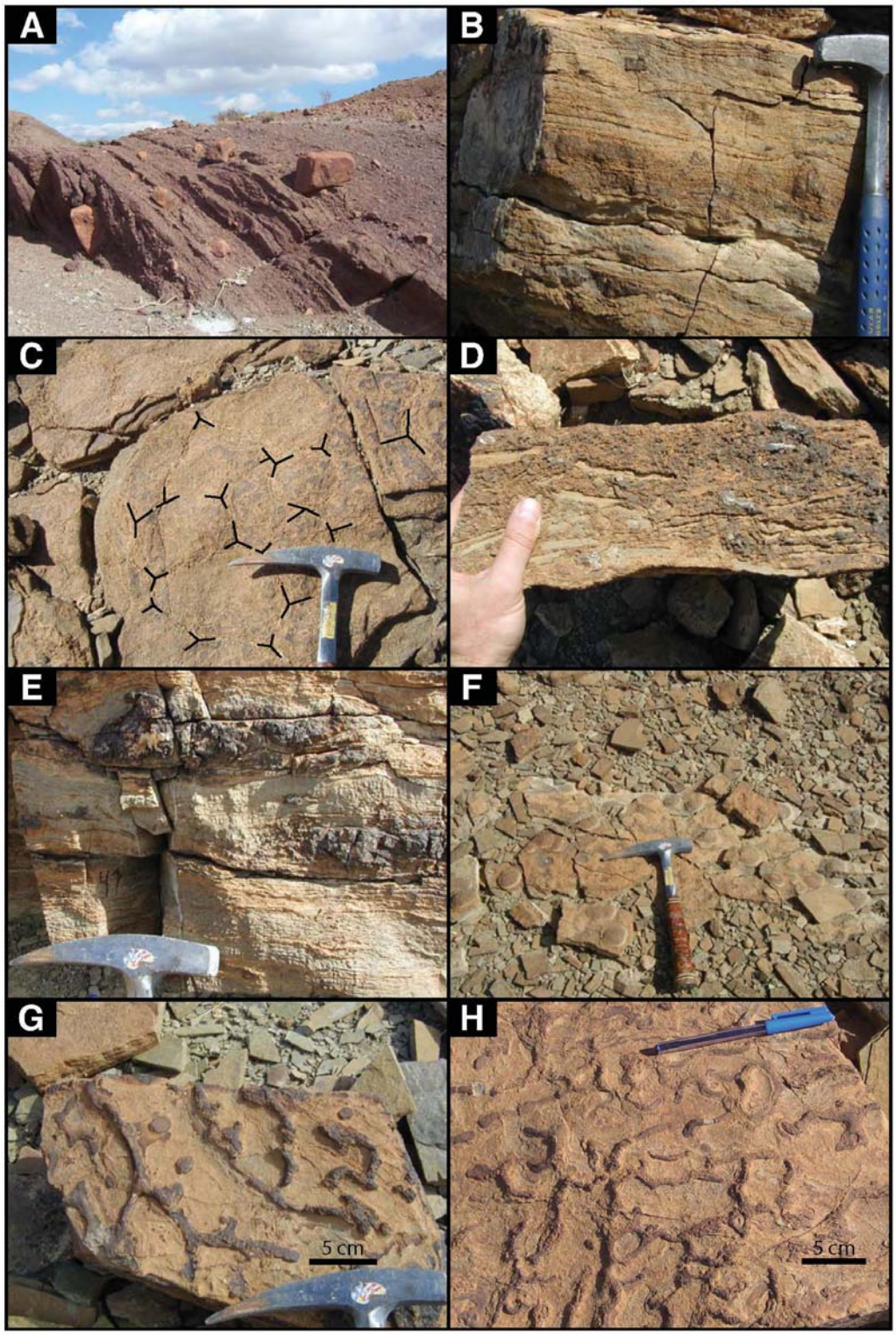

Figure 7. Mataar and Dhaiqa formation sedimentologic features. ***A.*** *Bedded polymict conglomerate of the Mataar formation, showing outsized subrounded boulders. The higher Mataar sequence (to the right of the image) grades into arkose and litharenite below initial limestone beds of the Dhaiqa formation. The boulder in the lower left of the photo is ~1 m long.* ***B.*** *Wavy and planar lamination in basal limestone of the lower Didikama Formation (close to sample 1). Relief differentiation appears to be partly related to differential growth of microbial mats (note partial chert replacement). Abundant "birdseye" fenestrae occur in thin section.* ***C.*** *Bedding plane view of desiccation cracks, indicating supratidal or shallow intertidal facies. Y-shaped marks are superimposed to emphasize polygonal joins.* ***D.*** *Intraclastic grainstone facies, indicative of a high-energy deposition (possible tempestite) above storm wave base. Micritic intraclasts show evidence of ductile deformation, indicating deposition prior to lithification.* ***E.*** *Planar and wavy microbialaminate facies (Sample 4). Differential weathering of algal (micropeloidal) layers and early diagenetic cement horizons ("birdseye" fenestrae) reveal algal mat textures. Stratiform chert nodules are common in this facies.* ***F.*** *Bedding plane view of microbialaminates (low relief laterally linked hemispheroids).* ***G–H.*** *Possible metazoan trace fossils observed in float from the dip slope of ridge 2 (see Figure 6). Horizontal traces showing bifurcation and looping. Burrows appear to be cylindrical in cross-section. Diameters are somewhat wider in* ***G****. Pen in* ***H*** *is 14 cm in length.*

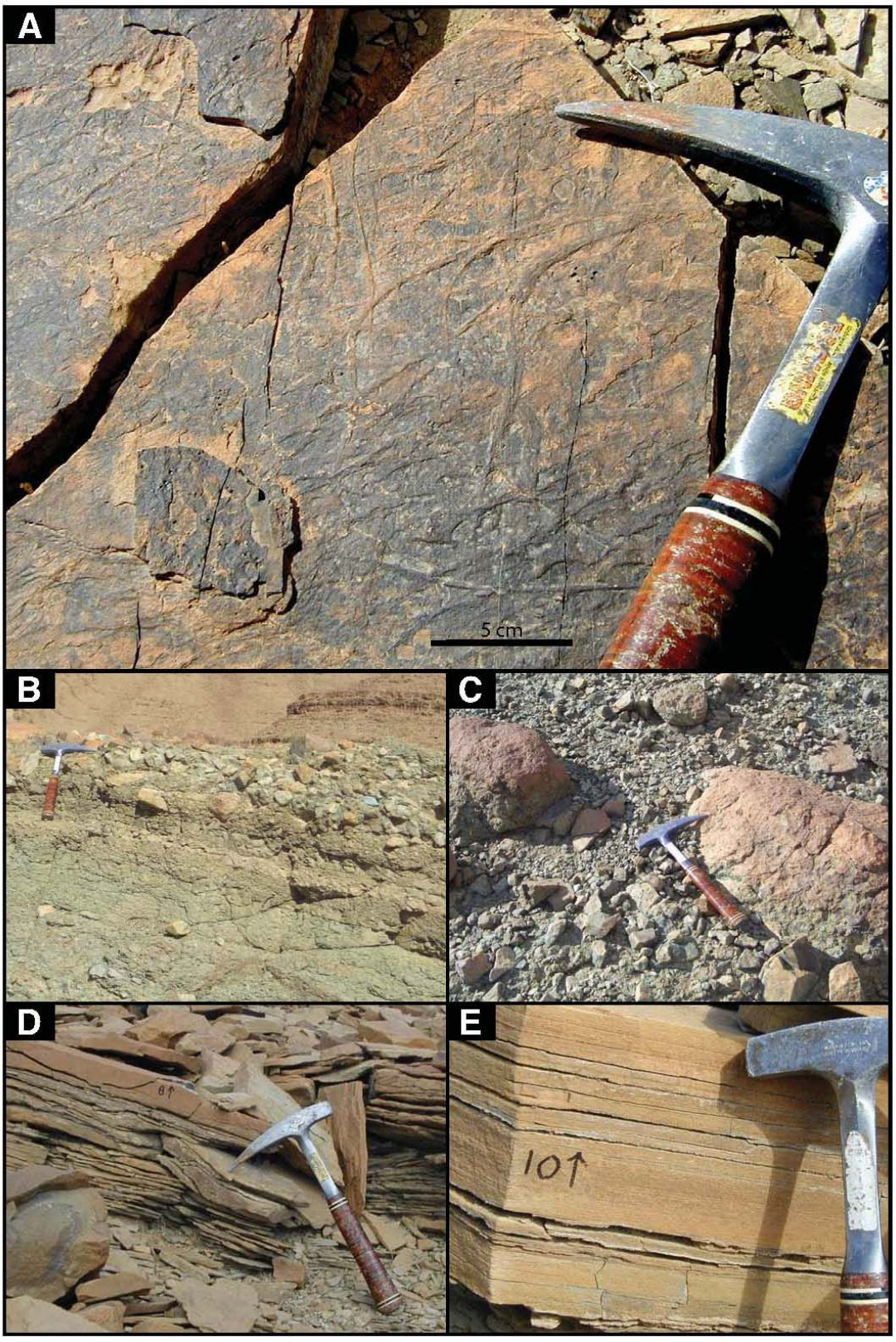

Figure 8. Dhaiqa formation sedimentologic features (continued). ***A.*** *Cross-cutting radiating structures of uncertain metazoan affinity (burrow traces or flattened strands/fronds?).* ***B.*** *Cross-sectional view of polymict conglomerate and underlying glauconitic arenite (sample 7a) from diamictite of the middle Dhaiqa formation (~180 m). Detrital zircons (± 10% discordant) from the lower glaucarenite facies (sample DY-1, see geochronology) range between 840 and 599 Ma. Outsized cobbles within the lower glaucarenite sequence, visible in the LL of the photo, may be dropstones.* ***C.*** *Top of polymict conglomerate showing large clasts (up to ~0.5 m).* ***D.*** *Thin flaggy algal wackestone (sample 8) from the upper Dhaiqa formation. Fine splitting may reflect weakness due to alternation of algal and clastic laminae.* ***E.*** *Fine parallel (<1mm) planar laminated algal wackestone facies (sample 10) from the top of the Dhaiqa formation transect.*

In the dip slope of the second ridge (Sample 6 and higher) are horizontal (bedding plane parallel) structures consistent with metazoan trace fossils. These were observed only in limestone float, and it is unclear whether the structures are from the tops or bottoms of bedding planes. Figure 7G–H shows apparent horizontal burrows that bifurcate and loop, found in two samples a few meters apart. The structures appear to be cylindrical with diameters on the order of 1 cm (Figure 7G) or somewhat less (Figure 7H). These morphologies suggest the activities of mobile animals with

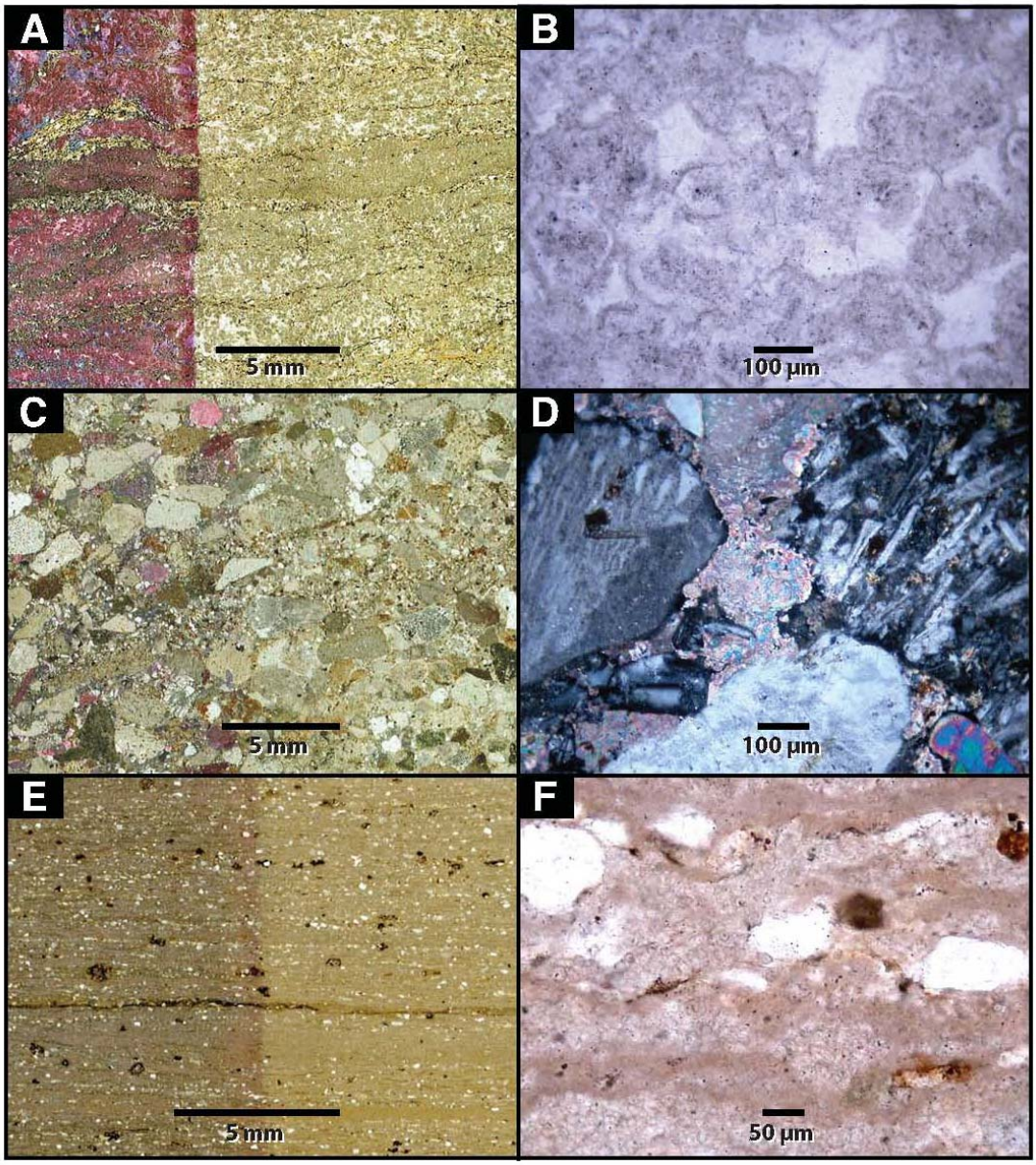

Figure 9. Petrographic views of Dhaiqa formation facies. ***A****. Microbial boundstone/grainstone (sample 4), showing darker comparatively organic-rich microbial laminae and lighter colored "birdseye" fenestral cements. Staining indicates late ferroan calcite spar cementation; scanned thin section.* ***B****. Close-up view of a calcite-cemented fenestral cavity in A, showing rimmed microbial peloids and encrusted filaments. Plane light with white card).* ***C****. Glaucarenite facies (sample 7a), below polymict conglomerate (~180m, see also Figure 7G), showing diverse grain compositions [chert, carbonate (pink), lithic fragments]; scanned thin section.* ***D)*** *Close-up view of C showing compositionally diverse grains (igneous and metamorphic) and matrix. Cross-polarized view.* ***E****. Finely laminated algal wackestone. Light colored stratiform grains are detrital silicate (mainly quartz and feldspar); scanned thin section.* ***F****. Close-up of fine micritic laminae in E. Plane light view with white card.*

digestive systems (worms?) living on or below the substrate. A different morphology shown in Figure 8A displays low relief radiating and crosscutting structures that seem inconsistent with inorganic chemical or physical processes (*e.g.*, cements, groove or tool marks). These structures can be traced laterally for 15 cm (or more), and are generally a few mm in width. They might be burrows, trails, or strands (radiating from a central area or holdfast or deposited separately).

Higher in the section (~180 m) carbonate deposition is interrupted by a distinct reverse graded 2-3 m thick sequence of glauconitic arenite followed by poorly sorted polymict conglomerate (Figure 8B). The green color of the composite interval makes it a distinctive marker bed. Clasts in the upper conglomeratic sequence range up to 0.5 m (Figure 8C). The sedimentary origin of this unit is unclear and we consequently term it a diamictite.

Carbonate deposition resumes abruptly over the diamictite sequence. The lowest bed consists of an algal boundstone (Sample 7b), with abundant peloids and late chert cement. Apart from its sharp basal contact, the bed lacked sedimentologic and geochemical characteristics of cap carbonates (*e.g.*, unusual textures or cements, teepee or roll-up structures, negative $\delta^{13}C_{carb}$ (*i.e.*, [26]). We found a large oncolite (~15 cm in diameter) with an igneous diamictite clast nucleus (~5 cm in diameter) in the float above the diamictite layer. This suggests that algal colonization directly ensued from diamictite deposition, and that moderate energy levels existed to move the accreting oncolite. The overlying carbonate sequence, examined in less detail, consists largely of flaggy (thin splitting) limestone beds with parallel laminations (Figure 8D–E). Petrographic inspection shows a prominent alternation of algal and detrital layers (rounded to subrounded quartz and feldspar), creating in some cases varve-like couplets (Figure 9E–F). We did not detect thicker stromatolitic biostromes, as observed in the lower Dhaiqa sequence.

4.2. Petrography

Dhaiqa formation limestones are principally boundstones, grainstones, or packstones in the lower portion of the unit, whereas laminated algal–clastic (varve-like wackestone) textures are more abundant higher in the uppermost part of the section. All samples are diagenetically altered to some extent, but primary depositional fabrics were discernable. Microbial boundstones reveal fabrics similar to modern marine stromatolites, including irregular alternation of concentrated algal material (intergrowths or layers of dark peloidal carbonate) and comparatively lighter early diagenetic cements (as uncompacted "birdseye" fenestrae; Figure 9A, B). Coarse-crystalline calcite and late ferroan calcite/dolomite cements (based on TS staining) occur in lower grainstones and microbialites, which may correspond to Mn and Fe enrichment (see below). Common traveling extinction patterns (suggesting botryoidal cementation) and prismatic textures in calcite are consistent with early marine-type cementation, although a saline lake could have similar mineralogies. Even the most "pure" carbonate samples have significant detrital mineral fractions, notably quartz, feldspar, and lithic fragments. Many silicate grains are well rounded and may not originate locally; or, if local, may be second cycle. Parallel laminated algal wackestone fabrics in the upper part of the section are well preserved, possibly due to lower initial porosities (Figure 9E, F). Petrographic inspection of glauconitic arenite from the conglomeratic interval (Sample 7*a*) reveals diverse (igneous, metamorphic, and sedimentary) grain compositions, including lithic fragments and limestone clasts (Figure 9C, D). Grains are rounded to subrounded. Carbonate cement is a ubiquitous component of the finer matrix.

4.3. Isotope and Trace Element Geochemistry

Geochemical results are reported in Table 1 and plotted in Figures 6, 10, 11. The acid soluble carbonate contents of samples are low averaging 40 ± 15%, reflecting appreciable chert content. $\delta^{13}C_{carb}$ ranges between –1.7 and +6.8‰ (Figure 6A), with an average of 2.4 ± 2.3‰. With two outliers (samples 4, 6), $\delta^{13}C_{carb}$ values are close to 2–3‰ for much of the Dhaiqa formation (Figure 6A dotted line); values become somewhat heavier in the upper part of the formation (Samples 8–10). $\delta^{18}O_{carb}$ ranges between -4.5 and -13.5‰, with an average of -10.4 ± 2.4‰. The lower 130 m of the formation shows a $\delta^{18}O_{carb}$ depletion trend from -9 to -14‰. Sample 7b, from limestone (< 1m) above the green diamictite layer has the highest $\delta^{18}O_{carb}$ (-4.5‰). Where samples were collected in close stratigraphic proximity (Samples 1, 2, 8–9) $\delta^{18}O_{carb}$ and $\delta^{13}C_{carb}$ compositions are comparable, suggesting that stratigraphic trends are preserved. Sr contents range from 559–3705 ppm (avg: 1448 ± 923 ppm) with corresponding $^{87}Sr/^{86}Sr$ between 0.70394-0.70603 (avg: 0.70501 ± 64), generally becoming more radiogenic upsection (Figure 6C). Mn/Sr and Fe/Sr average 1.5 ± 1.5 and 2.6 ± 1.6, respectively.

Table 1. Geochemical Data for Dhaiqa Formation Samples

Locality	Height (m)	Description	Petrographic Observations	Sampled Min	ASC* (%)	Fe (ppm)	Mn (ppm)	Sr (ppm)	Mn/Sr	Fe/Sr	$\delta^{13}C_{carb}$ (‰)	$\delta^{18}O_{carb}$ (‰)	$^{87}Sr/^{86}Sr$	2s error	reps
1	0	Peloidal grainstone/ packstone	Poor primary depositional fabric retention; highly cemented dark purple (Fe)	cal	17.9	3108	970	1205	5.3	2.0	1.4	–9.0	0.703944	± 22	2
2	4	Intraclastic grainstone	Poor, abundant late secondary Fe-rich spar, minor chert	cal	33.1	1673	482	560	0.8	1.4	1.8	–9.7	0.704166	± 16	2
3	67	Peloidal/ intraclastic grainstone	Poor but primary depositional texture evident. Late chert replacement; botryoidal fabric	cal	35.6	2401	329	559	0.7	1.5	2.0	–11.4	0.705426	± 24	2
4	86	Microbialaminite	Poor, late Fe-rich cement, but good primary fabric retention, clotted calcimicrobial textures (micropeloids) line stratiform fenestrae	cal	22.4	3404	1791	775	1.6	1.5	-1.7	–13.5	0.704429	± 22	2
5	101	Detrital wackestone	Massive-homogeneous texture; Abundant Fe-rich micrite, v. fine quartz detritus	cal	34.9	2600	624	1,543	1.4	4.0	2.1	–11.6	0.705139	± 23	2
6	120	Parallel laminated wackestone	Good primary fabric preservation; alternation of quartz-rich & micrite-rich layers	cal	36.7	5923	1998	1,476	0.4	1.7	6.8	–12.3	0.705071	± 19	2
7a	186	Glauconitic Ss, below diamictite	Microconglomerate, all grains <3mm; mix of rounded & angular; <10% carbonate grains, abundant glauconite & lithic fragments	Sample inappropriate for carbonate geochemical assessment											
7b	188	Algal boundstone	Moderate primary preservation, common organic/clayey seams; pod-like masses with micro-peloidal textures	cal	42.4	5475	5750	3705	2.3	4.4	1.2	–4.5	0.705157	± 28	2
8	279	Wackestone	Very fine grained homogeneous textured rock; abundant (20%) detritus as round to subrounded quartz & feldspar	cal	63.5	1898	816	1258	0.6	4.3	3.5	–10.7	0.706029	± 21	2
9	280	Laminated algal wackestone	Alternation of carbonate & detritus-rich layers on a sub-mm scale	cal	64.9	1874	1064	1302	0.9	3.0	2.8	–9.8	0.705356	± 19	2
10	293	Laminated algal wackestone	Very good primary laminated texture, detritus defines layers; lots of fine opaque clusters (pyr?).	cal	43.7	4163	11090	2098	0.8	2.6	4.7	–11.0	0.705354	± 34	3

*ASC = 0.8M acetic acid-soluble carbonate content in percent

4.4. Diamictite Geochronology

As mentioned above, the Dhaiqa formation is directly dated by detrital zircons extracted from fine-grained green sandstone (DY-1) from the middle part of the limestone succession, but because this is the only sample, to date, the results are treated as a preliminary, not definitive, indication of the maximum deposition age. The zircons are commonly fragmented and rounded as is typical of detrital grains (Figure 11A-B, E). Morphologies include a mix of large striped and oscillatory-zoned zircons lacking overgrowths, and more equant zircons with well developed overgrowth rims up to 50 µm wide. High and low U contents were measured among the rimmed zircons. Because the Dhaiqa formation is neither metamorphosed nor obviously affected by hydrothermal fluids, it is inferred that the zircon overgrowths developed in the source rocks prior to their erosion and extraction as detrital grains; although zircon rims may grow *in situ* at relatively low temperatures, and growth following deposition cannot be definitively discounted. Together, the combination of varied morphologies and rim-U contents suggest detrital derivation from different sources. Twenty-four spots were analyzed (Table 2). The age data spread along the concordia from approximately 900 Ma to 400 Ma (Figure 11C). There is evidence of resetting of ages in high-U zircons and in the cores of zircons with cracking; the youngest ages are from the cracked regions of zircon cores. The relative probability diagram (Figure 11D) has a maximum at approximately 610 Ma, representing the age of the largest component of zircons in the sample. For greater robustness, Figure 11F is a histogram of $^{206}Pb/^{238}U$ ages that are within ±10% concordance, corrected using ^{204}Pb. This plot indicates minimum ages in the 570-600 Ma range. The youngest ages in the data set are from the core (599 ± 4.8 Ma) and rim (570 ± 4.6 Ma) of a single grain (top left-hand corner of Figure 11E). Because both of these ages occur in the same grain and we have a limited set of observations from which to judge rim/core/[U] age relationships, the significance of the rim versus core age is unclear. Because we cannot exclude the possibility that the rim could reflect a reset age similar to the younger cores of some cracked zircon grains or a post-depositional growth age, we tentatively consider both dates as possible maximum age constraints. The diamictite (and probably the entire Dhaiqa formation) must be younger than 599 ± 4.8 Ma, but could very well be younger than 570 ± 4.6 Ma. Both ages are consistent with the Ediacaran age inferred for the formation on general geologic evidence.

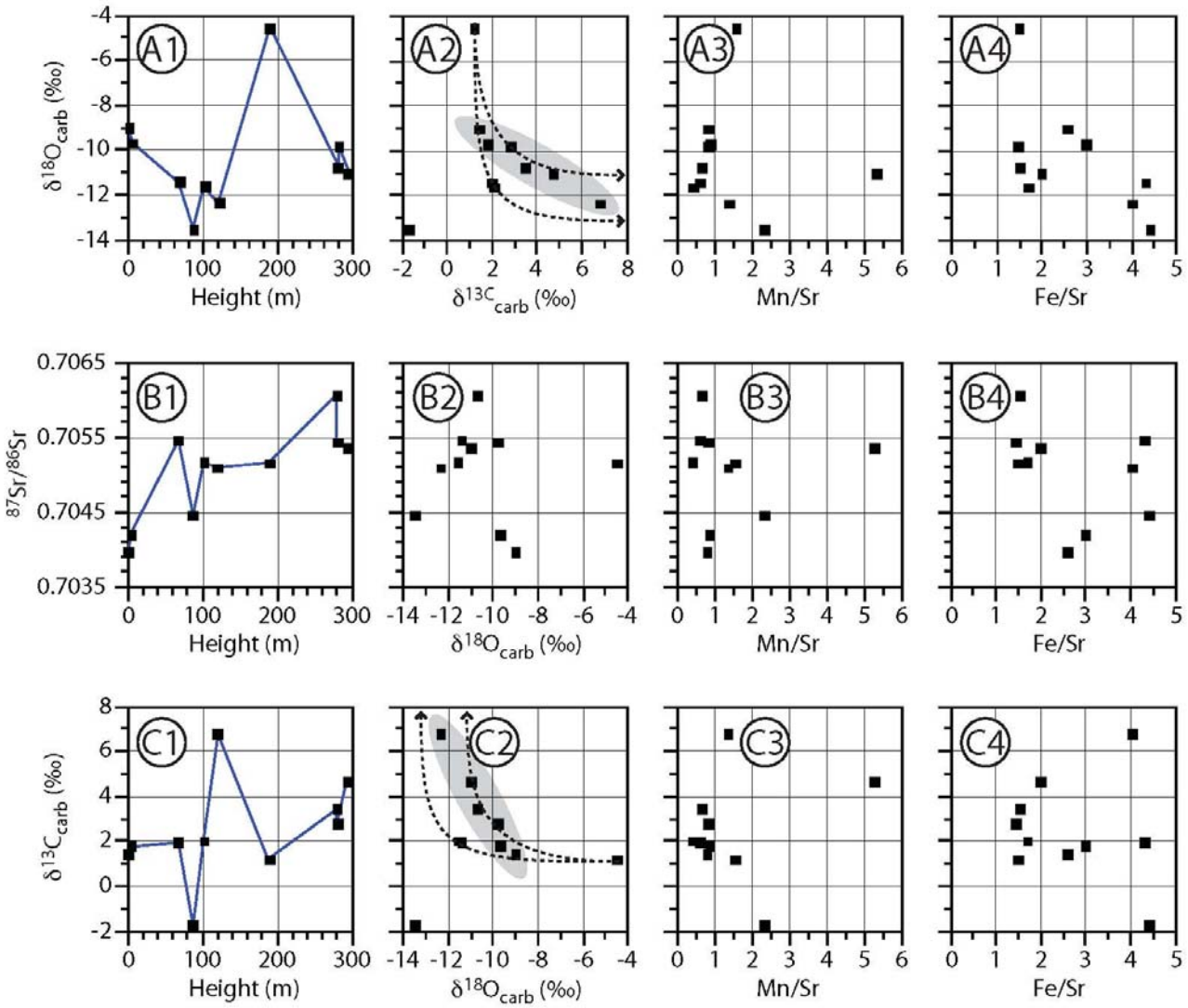

Figure 10. Evaluation of $\delta^{18}O_{carb}$ ***(A1-4)****, $^{87}Sr/^{86}Sr$* ***(B1-4)****, and $\delta^{13}C_{carb}$* ***(C1-4)*** *diagenesis. Each series plots y-axis parameter variance versus stratigraphic position, $\delta^{18}O_{carb}$ (or $\delta^{13}C_{carb}$), Mn/Sr, and Fe/Sr. Shaded ellipses in* ***A2*** *and* ***C2*** *show a possible correlation trend indicative of diagenetic alteration. Dashed arrows in* ***A2*** *and* ***C2*** *show idealized fluid-rock alteration paths; arrows point in the direction of progressive alteration. See Table 1 for data.*

5. DISCUSSION

5.1. Sample Preservation

Ancient carbonates always undergo diagenesis to some extent (recrystallization, dolomitization, *etc*.) and this can alter isotopic compositions from primary depositional values. The Ediacaran Period (630–542 Ma) has reasonably well-constrained $\delta^{13}C_{carb}$ and $^{87}Sr/^{86}Sr$ records [10,5, 27,28,] that can be used to help interpret the Dhaiqa formation data (Figure 12). Oxygen isotopic compositions of Ediacaran marine carbonates are generally depleted relative to those of Phanerozoic marine carbonates, but the Ediacaran Period falls within a 750–500 Ma interval characterized by high $\delta^{18}O_{carb}$ variability (0 to –20‰, or lower) and poor age control [29,30]. Thus, there is not a robust empirical basis for interpreting Ediacaran $\delta^{18}O_{carb}$ records. Water-rock modeling predict increasing relative susceptibility to diagenetic alteration in the series: $\delta^{18}O_{carb}$, $^{87}Sr/^{86}Sr$, and $\delta^{13}C_{carb}$ [31,32,29]. Petrographic inspection indicates that most Dhaiqa formation samples contain secondary calcite and late ferroan calcite (or dolomite), and a significant chert component. These secondary phases indicate active fluid–rock interaction.

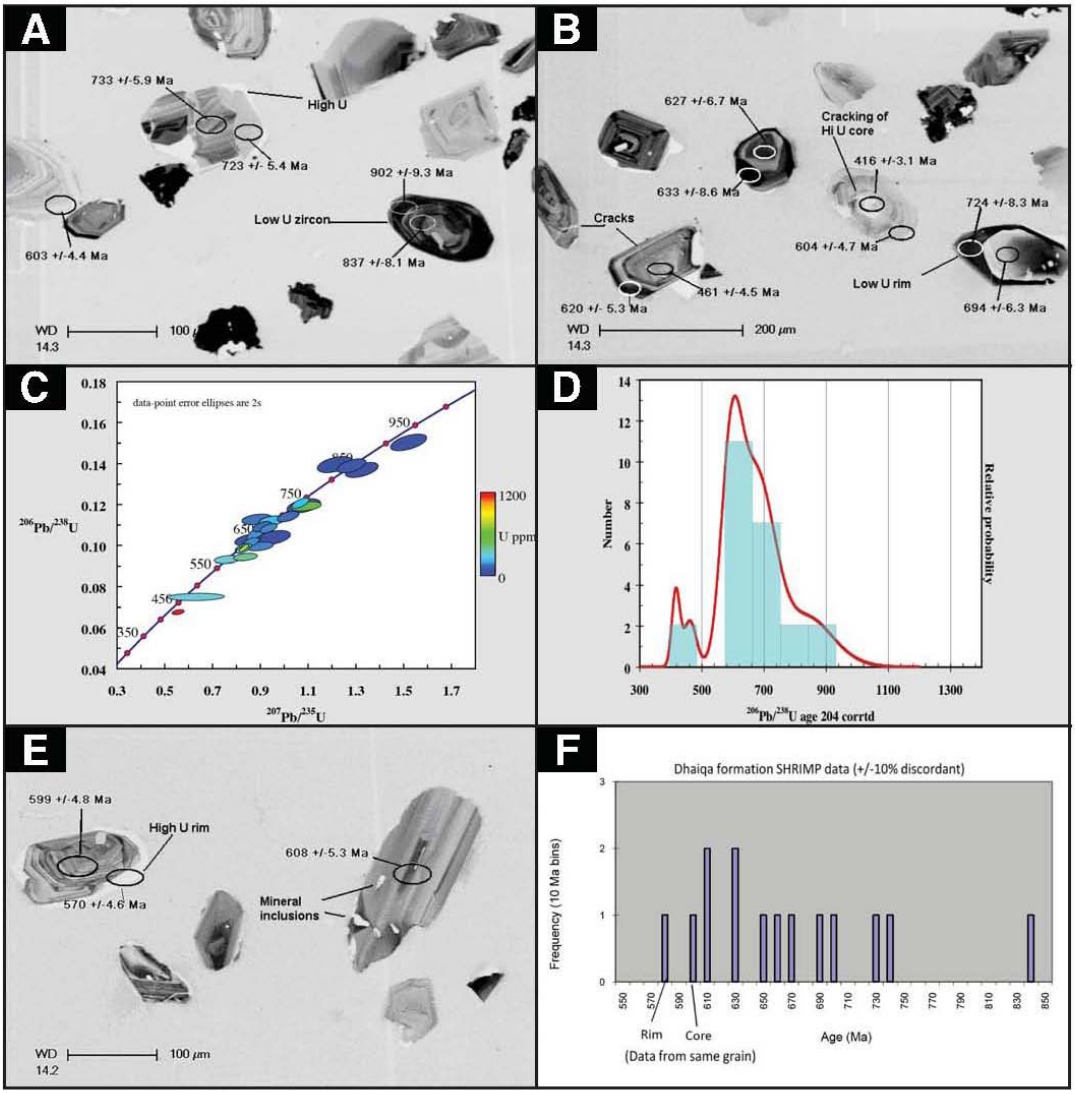

Figure 11. Zircon images and SHRIMP U-Pb geochronology summary plots for the Dhaiqa formation diamictite (see Figure 3). ***A-B, E****. CL negative images of sample DY-1 zircons, showing core and rim age variations.* ***C****. Concordia diagram for DY-1 zircons.* ***D****. Relative probability plot for DY-1 zircons.* ***F****. Histogram age distribution for DY-1 zircons (±10% discordant).*

The strontium isotope range (0.7039–0.7060) in these samples is well below that reported for Ediacaran marine values (Figure 12; 0.7063-0.7087) [28,10]. Values as low as 0.7039 demonstrate a significant source of juvenile ensimatic Sr, that is, Sr in the carbonates was derived from igneous rocks recently melted from the mantle. This juvenile Sr could have resulted from diagenesis or deposition in a restricted basin. The stratigraphic increase in $^{87}Sr/^{86}Sr$ (Figure 10-B1) may indicate a lessening of this influence through time. The association of Jibalah Group basins with extensional tectonics [17,33] could indicate that the Dhaiqa Basin was controlled by faults, along which crustal fluids could have entered. Alternatively, if the Dhaiqa Basin was essentially a down-faulted graben, chemical weathering of older Neoproterozoic juvenile crust could have provided runoff with highly unradiogenic Sr, which controlled the Sr isotopic composition of lacustrine or estuarine waters. The persistence of fine detritus in Dhaiqa formation samples suggests a setting that was likely not far-removed from emergent source areas. The fine layering may indicate seasonal control of detrital input, possibly changing runoff or eolian input to the basin.

The influence of diagenetic fluids on marine carbonate preservation is often evaluated by comparing $\delta^{18}O_{carb}$ to $\delta^{13}C_{carb}$, or these with Mn/Sr, Fe/Sr, $^{87}Sr/^{86}Sr$, or other geochemical proxies [32,34]. A crossplot of $\delta^{18}O_{carb}$ *vs.* $\delta^{13}C_{carb}$, shown in Figure 10-A2 (and C2) suggests a trend of decreasing $\delta^{18}O_{carb}$ with increasing $\delta^{13}C_{carb}$. Two outlying samples

from this trend, with extreme $\delta^{18}O_{carb}$ compositions, may indicate isotopic exchange during replacement. The trend could indicate that least altered Dhaiqa formation samples have $\delta^{13}C_{carb}$ near 2‰ and $\delta^{18}O_{carb}$ in the range of –9 to –12‰. This trend corresponds to samples with lowest Mn/Sr (<1) and less precisely to lowest Fe/Sr (<3). Applying these Mn/Sr and Fe/Sr bounds to $\delta^{13}C_{carb}$ suggests least altered compositions between 1 and 4.7‰, and thus deposition from basin waters having positive $\delta^{13}C_{DIC}$. We note that highest $^{87}Sr/^{86}Sr$ compositions (most likely to be least altered if marine) generally correspond to samples with lowest Mn/Sr and Fe/Sr. These observations make it difficult to claim that Dhaiqa isotopic compositions reflect the composition of the waters in which they were deposited, with the possible exception of $\delta^{13}C_{carb}$ (dotted line in Figure 6).

Table 2. Geochronology Data for Dhaiqa Formation Diamictite (DY-1)

Spot	% $^{206}Pb_c$	ppm U	ppm $^{206}Pb^*$	$^{232}Th/^{238}U$	±%	(1) $^{206}Pb/^{238}U$ Age	(2) $^{206}Pb/^{238}U$ Age	(1) $^{207}Pb/^{206}Pb$ Age	(2) $^{207}Pb/^{206}Pb$ Age	% Dis-cor dant
DY-1-1	--	163	14.1	0.565	0.4	621 ±5.3	623 ±1.1	655 ±29	588 ±10	5
DY-1-2	3.96	284	18.1	0.913	0.3	462 ±4.5	487 ±1.1	632 ±169	296 ±20	28
DY-1-3	--	32	2.8	0.591	0.9	633 ±8.6	627 ±2.2	819 ±61	703 ±25	24
DY-1-4	--	57	5.01	0.618	0.6	627 ±6.7	629 ±1.7	592 ±54	609 ±17	–6
DY-1-5	0.87	1164	66.7	2.569	0.3	417 ±3.1	531 ±3.2	586 ±38	221 ±5	30
DY-1-6	0.02	377	31.8	0.603	0.3	605 ±4.7	609 ±0.9	631 ±30	560 ±9	4
DY-1-7	--	50	5.08	0.294	0.7	725 ±8.3	725 ±1.4	794 ±50	721 ±27	9
DY-1-8	--	121	11.8	0.326	0.5	694 ±6.3	694 ±1.1	758 ±34	692 ±17	9
DY-1-9	--	160	14.8	0.35	0.4	660 ±5.6	660 ±1.0	689 ±28	676 ±13	4
DY-1-10	0.60	134	12.9	0.383	0.4	686 ±6.1	691 ±1.1	483 ±63	597 ±23	–44
DY-1-11	0.14	200	19.2	0.242	0.3	683 ±5.6	684 ±0.9	646 ±48	641 ±30	–6
DY-1-12	--	771	65	0.294	0.2	603 ±4.4	603 ±0.7	638 ±14	607 ±7	6
DY-1-13	--	211	21.8	0.73	0.3	733 ±5.9	734 ±1.4	743 ±23	729 ±10	1
DY-1-14	0.68	510	52	0.136	0.2	724 ±5.4	723 ±1.0	816 ±48	774 ±48	12
DY-1-15	0.01	81	9.65	0.458	0.5	837 ±8.2	838 ±1.7	833 ±35	821 ±18	–1
DY-1-16	--	66	8.53	0.467	0.6	903 ±9.3	898 ±2.0	1021 ±34	969 ±23	12
DY-1-17	0.41	53	6.37	0.383	0.7	841 ±9.1	845 ±1.8	704 ±47	771 ±23	–21
DY-1-18	--	57	6.66	0.263	0.6	826 ±8.6	822 ±1.5	930 ±37	949 ±29	12
DY-1-19	0.04	126	11.7	0.421	0.4	666 ±5.9	666 ±1.1	608 ±34	658 ±14	–10
DY-1-20	--	165	15	0.242	0.4	649 ±9.0	650 ±0.9	614 ±30	621 ±16	–6
DY-1-21	0.51	390	31.4	0.906	0.2	578 ±4.5	577 ±1.2	750 ±50	580 ±10	24
DY-1-22	0.12	156	13.3	0.572	0.4	609 ±5.3	603 ±1.2	783 ±53	668 ±17	23
DY-1-23	--	245	20.5	0.278	0.3	600 ±4.8	601 ±0.7	642 ±26	576 ±11	7
DY-1-24	0.26	283	22.5	0.265	0.3	571 ±4.6	576 ±0.7	572 ±61	433 ±28	0

Errors are 1-sigma; Pbc and Pb* indicate the common and radiogenic portions, respectively.
Error in Standard calibration was 1.44%
(not included in above errors but required when comparing data from different mounts).
(1) Common Pb corrected using measured ^{204}Pb.
(2) Common Pb corrected by assuming $^{206}Pb/^{238}U$–$^{208}Pb/^{232}Th$ age-concordance

5.2. Was the Dhaiqa Basin Marine?

Whether or not the Dhaiqa formation is marine requires further study of Dhaiqa basin and other Jibalah Group basins with carbonate successions from the NW Arabian shield. The Dhaiqa formation overall appears to preserve a deepening upward sequence that could record a marine transgression or tectonic basin subsidence, the latter in either a marine or non-marine setting. A lack of Dhaiqa equivalents regionally could reflect the diversity of sedimentological influences during the Ediacaran Period or a preservational bias related to the timing and magnitude of basin subsidence. Stromatolitic structures are similar in lake and marine strata and thick carbonates are common in ancient lake deposits (*e.g.*, Green River Shale, which is predominantly carbonate; A. Brown, personal communication). The very unradiogenic Sr isotope compositions in the Dhaiqa formation could reflect retention of primary values in a lacustrine setting dominated by ensimatic Sr input, or extreme alteration of primary marine compositions. Certainly the high Sr content of Dhaiqa formation carbonate suggests the measured $^{87}Sr/^{86}Sr$ are primary. Regardless, it is difficult to explain how apparently marine $\delta^{18}O_{carb}$ values could be preserved if $^{87}Sr/^{86}Sr$ is altered, and the trace element data do support a possible diagenetic end-member fluid with $\delta^{18}O$ between –11 and –13‰ (section 6.1). This leaves only $\delta^{13}C_{carb}$ as a possibly reliable seawater proxy.

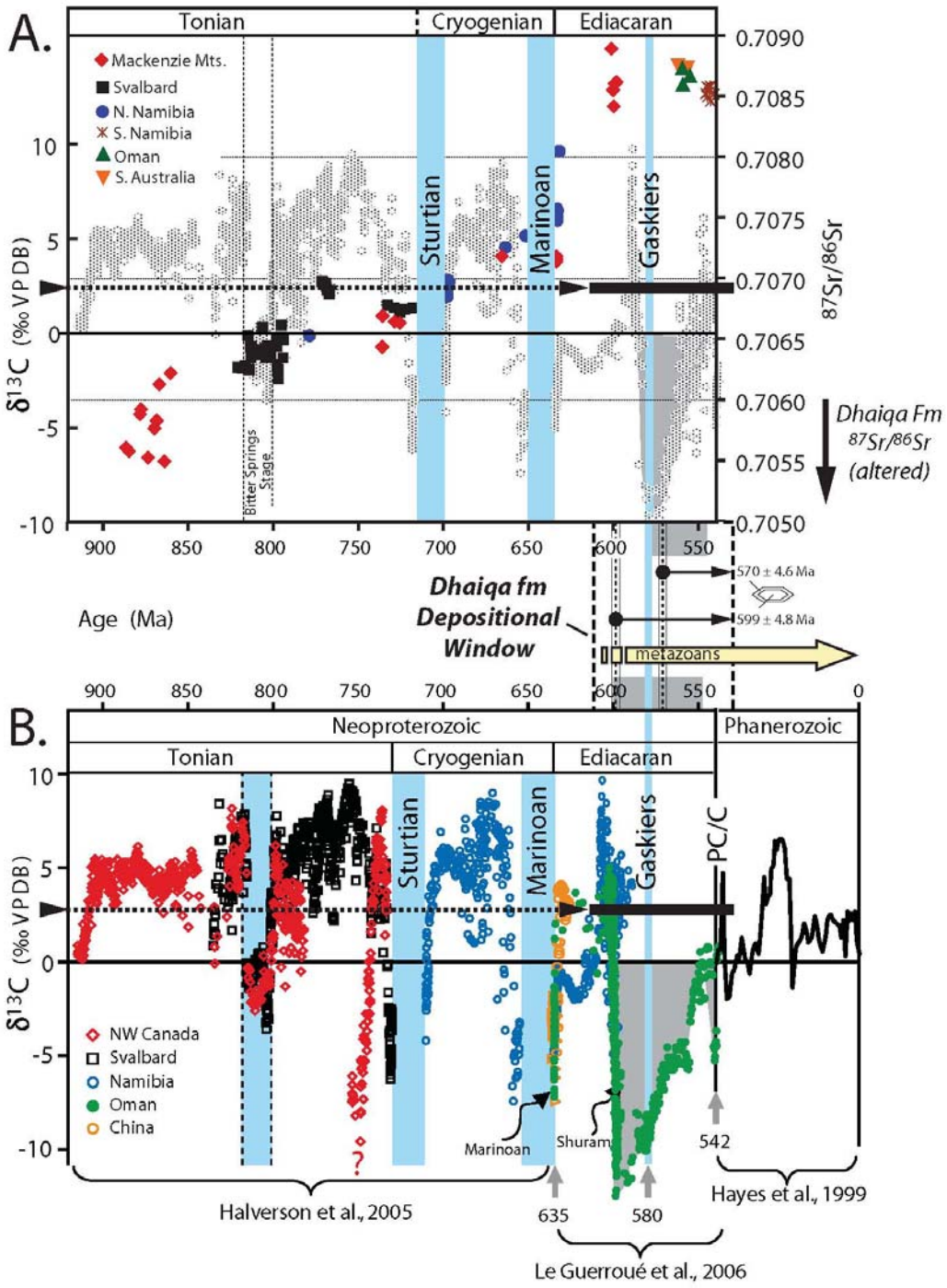

Figure 12. ***A****. Summary plot of Neoproterozoic $\delta^{13}C_{carb}$ and $^{87}Sr/^{86}Sr$ variation in shallow marine carbonates from Halverson et al. [28]. Sr-isotope data are emphasized (color symbols) over C-isotope data (small gray dots).* ***B****. Neoproterozoic and Phanerozoic $\delta^{13}C_{carb}$ from Le Guerroué et al. [10], as modified from Halverson et al. [28] and Hayes et al. [46]. Neoproterozoic carbon isotope data are the same between the two plots, but note that two different age models apply to the age and duration of the Shuram negative $\delta^{13}C_{carb}$ anomaly within the Ediacaran Period, shown as upper and lower gray boxes in the Dhaiqa formation depositional window. The upper box corresponds to the age model of Fike et al [5]; the lower box to that by Le Guérroue et al. [10] (see text for elaboration). The position of the Gaskiers glaciation relative to the Shuram anomaly varies significantly between the two age models. The two dashed intervals within the Dhaiqa formation depositional window show competing minimum ages obtained from the same zircon grain (core: 599 ± 4.8 Ma; rim: 570 ± 4.6 Ma).*

The case for a marine depositional setting is best supported by the following arguments. Since definitive non-marine Ediacaran fauna have not been reported (A. Knoll, personal communication), confirmation of the putative metazoan trace fossils would suggest a marine association. Nevertheless, the possibility that Ediacaran metazoans lived in lacustrine or estuarine environments cannot be dismissed. Recognition of separate Jibalah Group basins having common carbonate stratigraphies and chemostratigraphies would enhance the case for a widespread marine depositional setting. This may be seen further east and south in the Arabian Platform, where the Jibalah Group may correlate to the Nafun Group of Oman [13]. Below the ~520 Ma base-Phanerozoic unconformity, both groups are overlain by salt-bearing groups (subsurface only and unnamed in Saudi Arabia; Ara Group in Oman). Allen [18] notes that widespread lithostratigraphic correlations are possible throughout the ~1 km thick Nafun Group, and suggests that deposition occurred within a continental margin sag basin that extended NE into a passive continental margin setting within the eastern (tectonically deformed) periphery of the ANS. Extensional collapse and tectonic escape may have facilitated regional subsidence and creation of the greater Nafun-Jibalah basin, leading to widespread marine inundation of the Arabian shield area [18]. Organic geochemistry of the Nafun Group also provides evidence for marine deposition that could extend regionally to include Jibalah Group basins. Specifically, a marine algal biomarker (isomers of 24-*n*-propylcholestane, which are C30 steranes derived from marine pelagophyte algae) is detected throughout the Huqf Supergroup in the South Oman Salt Basin, including the Nafun Group [35; G. Love, personal communication].

Another perspective on the depositional environment comes from the Mataar formation, which appears to be fluvial or glacial in origin with no evidence for deposition in a marine environment. The clast assemblage is similar to that of fluvial sediments of <585 ± 13 Ma Hammamat sediments [36] and/or the >595 ± 2 Ma Saramuj Conglomerate of Jordan [37], and the possibility that the Mataar–Saramuj–Hammamat are parts of a single, integrated terrestrial drainage basin should be investigated. It is thus probable that the Dhaiqa basin began as a nonmarine basin but whether or not this setting persisted throughout Dhaiqa formation deposition is not known.

5.3. Age, Glacial Association, and Possible Relation to Oman Lithostratigraphy

Local and regional stratigraphic relationships (described in the geologic setting) establish that the Dhaiqa formation is between 609–530 Ma, regardless of its depositional setting. Concordant (within 10%) detrital zircons in the Dhaiqa diamictite indicate that Dhaiqa formation is younger than 599 ± 4.8 Ma and/or 570 ± 4.6 Ma. If the Dhaiqa diamictite interval (Figure 6, 8B-C) is glacial, the ~580 Ma Gaskiers glaciation [38] is an obvious candidate compatible with the older maximum zircon age estimate, but cannot be accommodated by the younger zircon age. Prospective glacial deposits (dropstones) also occur in the Jifn Basin in the NE Arabian shield [33; their Figure 7D]. Here, the Jibalah Group consists of a 3 km thick succession of conglomerate, limestone, sandstone, and shale. U–Pb zircon dates constrain deposition between 625 ± 4 Ma and 576.6 ± 5.3 Ma, and thus the Jibalah Group in the Jifn Basin may have spanned the interval of Gaskiers glaciation. These observations suggest that ~580 Ma could be a pinning point within the suggested 599-530 Ma depositional window for the Dhaiqa formation. An alternative interpretation feasible from the younger 570 ± 4.6 Ma Dhaiqa diamictite zircon age is that the Dhaiqa Formation is entirely younger than the Gaskiers glaciation and that the Dhaiqa diamictite corresponds to another glaciation or was deposited independent of glacial processes. Although not required, the underlying Mataar formation with its outsized boulders (Figure 7A) and regional age relations indicating it is younger than 609 Ma but older than the youngest Dhaiqa diamictite zircon, could be a candidate for the Gaskiers glaciation.

Further age constraints are possible from the Dhaiqa $\delta^{13}C_{carb}$ record, assuming it is marine and not highly altered. Figure 12 shows Neoproterozoic $\delta^{13}C_{carb}$ variations as modified from Halverson et al. [28: Figure 12A] and Le Guerroué et al. [10: Figure 12B] with the intersection of modal Dhaiqa formation $\delta^{13}C_{carb}$ values for the 609-530 Ma depositional window (shown as horizontal black bars). With minor variations, pre-Ediacaran $\delta^{13}C_{carb}$ data (grayed out in figure 12A by [28] to emphasize $^{87}Sr/^{86}Sr$ variation) are the same. Figure 12B emphasizes Ediacaran $\delta^{13}C_{carb}$ outcrop and subcrop data from the Huqf Supergroup of Oman [10]. Age models for the Ediacaran $\delta^{13}C_{carb}$ data vary appreciably between the plots (further discussed below), but the major isotopic trends are comparable. Of obvious significance is the pronounced negative $\delta^{13}C_{carb}$ anomaly that dominates much of the Ediacaran marine record. The anomaly is known in Death Valley, S. Australia (called the Wonoka anomaly), and S. China, but has been studied in greatest detail from Oman (Nafun Group, Huqf Supergroup) [39,40,27,10,5] and we consequently refer to this as the Shuram anomaly. In fact, the Shuram anomaly is the single greatest $\delta^{13}C$ excursion of Neoproterozoic time. The tentative Dhaiqa formation depositional window, superimposed between the two Figure 12 plots, spans the Shuram anomaly (shown as grey boxes extended from the bounding plots). Given the predominance of positive $\delta^{13}C_{carb}$ values, Dhaiqa formation deposition–if marine–must have either preceded or followed the Shuram anomaly. The age of the Shuram anomaly could therefore potentially further constrain the Dhaiqa formation depositional window.

In Oman (Nafun Group, Huqf Supergroup) negative $\delta^{13}C_{carb}$ compositions of the Shuram excursion begin above a local unconformity between the Khufai and Shuram Formations [5]. Detrital zircons are older than 620–600 Ma in the uppermost Khufai Formation [10,41]; thus the base of the Shuram anomaly must be younger. Le Guerroué *et al*. [10] used a subsidence model to estimate formational boundary ages, from which they interpret the Shuram anomaly to initiate at ~600 Ma. On the basis of sequence stratigraphic correlation, Fike *et al*. [5] match the unconformity to the Gaskiers glaciation (~580 Ma), with negative $\delta^{13}C_{carb}$ values beginning above 6m in the Shuram Formation (with a speculated age of ~570–560 Ma, see [5,41]). Thus, the onset age of Shuram anomaly negative $\delta^{13}C_{carb}$ compositions varies by 30–40 million years between these two age models, with no direct dates. Carbon isotope values next become positive in the overlying Buah Formation and positive values continue until a small negative excursion (–3‰) is encountered at the Precambrian–Cambrian boundary in the Ara Group [42]. The recovery to positive values in the mid-Buah Formation can be placed at 551.1 ± 0.7 Ma (based on correlation with Douschantuo Formation, China [43]) and Ara Group deposition was ongoing from ~547 through ~541 Ma [42,41]. Thus both age models are in reasonable agreement that the Shuram negative $\delta^{13}C$ excursion ended about 551 Ma (>547 Ma–Ara Group) and was followed by positive values until the Precambrian–Cambrian boundary (within the Ara Group).

Based on the available age constraints for the Shuram anomaly, the positive $\delta^{13}C_{carb}$ values measured for the Dhaiqa formation could correspond to: (1) the pre-Shuram interval (Khufai Formation), either > 600 Ma [2] or > 570–560 Ma (some time shortly following the ~580 Ma Gaskiers glaciation [10]); or (2) the post-Shuram interval (Buah and Ara Groups) between ~551–542 Ma. The combination of the 609 Ma basal age constraint for the Mataar-Dhaiqa formation interval and the occurrence of 599 ± 4.8 Ma detrital zircons in the Dhaiqa formation diamictite (if this is superior minimum zircon age) are compatible with the Shuram anomaly initiating at either of the model ages [10,5]. However, only the Fike *et al*. [5] age model specifies positive $\delta^{13}C_{carb}$ compositions through the Gaskiers interval, prior to the Shuram anomaly, that could support either the Mataar formation or Dhaiqa diamictite as a Gaskiers correlate; the Le Guérroue *et al.* [10] age model predicts negative $\delta^{13}C_{carb}$ compositions for the Gaskiers interval within the Shuram anomaly. Interestingly, the Khufai Formation has an average $\delta^{13}C_{carb}$ composition (2.4 ± 0.9‰, n = 34, [5]) identical to that for the Dhaiqa formation (2.4 ± 2.3‰, n = 10). The corresponding comparison with $\delta^{18}O_{carb}$ is –7.1 *vs*. -10.4‰. If the superior minimum zircon age for the Dhaiqa diamictite is 570 ± 4.6 Ma, only the Fike *et al*. [5] age model could still support a pre-Shuram anomaly correlation on the basis of $\delta^{13}C_{carb}$, but this age constraint excludes any correlation with the Gaskiers glaciation. The Buah Formation overlying the negative Shuram anomaly has $\delta^{13}C_{carb}$ and $\delta^{18}O_{carb}$ averaging 3.8± 2.3‰ and -0.6± 1.0‰, respectively; n = 22, [5]. Both age models accommodate a post-Shuram anomaly correlation with the Dhaiqa formation, implying the Dhaiqa formation could be younger than ~551 Ma with no Gaskiers glacial interval. Although the possible association of either the Mataar formation or Dhaiqa diamictite with the Gaskiers glacial could support a pre-Shuram correlation with the Khufai Formation, the Dhaiqa formation stable isotope statistics are not particularly robust compared to the alternative correlation with the post-Shuram Buah Formation and Ara Group. Accordingly, we cannot confidently assign the Dhaiqa formation with respect to the Shuram anomaly.

5.4. Implications of Ediacaran Metazoan Fossils

If the Dhaiqa formation is marine and retains marine $\delta^{13}C_{carb}$ compositions, its putative metazoan trace fossils must date before or after the Shuram anomaly. As discussed above, the onset age of the Shuram anomaly and the maximum age of the Dhaiqa diamictite (~599 vs. 570 Ma) are unresolved, and the combination of Dhaiqa formation age constraints and positive $\delta^{13}C_{carb}$ compositions can only accommodate the pre-Shuram age model of Fike *et al*. [5]. The occurrence of the traces below the Dhaiqa diamictite could mean they are older than ~580 Ma, if the diamictite is Gaskiers. The discovery of unambiguous metazoan burrows older than 580 Ma, regardless of paleoenvironment, would be news. Unambiguously non-marine Ediacaran animals have not been reported; most or all come from successions with undisputed marine origins. Ediacaran fossils have been found in carbonates in northern Siberia, and there is some evidence of burrowing in <549 Ma carbonates of the Nama Group, Namibia. However, behaviorally complex or deeply penetrating burrowers are not recorded until the very end of the Ediacaran Period (A. Knoll, personal communication). The latter observations would tend to support a correlation of the Dhaiqa formation within the ~551–542 Ma post-Shuram recovery interval (uppermost Nafun (Buah Formation) and Ara Group).

Warm and saline oceans for most of the Precambrian, with correspondingly limited O_2 solubilities, may have precluded an earlier rise of metazoans, with their increased demands for oxygenic respiration. Less saline and cooler oceans with O_2 solubilities high enough to support the rise and global proliferation of Ediacaran metazoans may have ensued following widespread deposition of evaporites ('saline giants') at the end of the Neoproterozoic, perhaps aided by earlier cooling from Cryogenian glaciations [44]. Prior to this, non-marine environments (lagoons, lakes, estuaries) could have been sufficiently oxygenated to permit the rise of metazoans [44]. Post-Shuram excursion Ara Group evaporites of

the Oman salt basins constitute one of these latest Neoproterozoic 'saline giants' [45]. More work is required to resolve the marine *versus* non-marine depositional setting of the Dhaiqa formation, its timing relative to deposition of Ara Group evaporites, and the authenticity of metazoan trace fossils, but these observations suggest that there could be important implications for metazoan diversification and radiation.

5.5. Implications for Timing of Najd Deformation

Movement along the Najd fault system probably deformed sediments of the Dhaiqa formation. The inferred depositional age of <599 ± 4.8 Ma or <570 ± 4.6 Ma, coupled with the fact that these sediments are deformed, implies that Najd activity continued until at least this time.

6. CONCLUSIONS

The Dhaiqa formation was deposited between ≤ 600 Ma and ~530 Ma in a shallow, relatively energetic, aqueous setting that deepened and quieted through time. Sedimentary facies grade upward, from supratidal and intertidal algal boundstones and grainstones, into quieter parallel-laminated algal wackestones. The continuity of predominantly carbonate deposition was interrupted by a diamictite unit with concordant zircons as young as 599 ± 4.8 (core) and/or 570 ± 4.6 (rim) Ma. The likely occurrence of metazoan trace fossils, if confirmed, in addition to positive $\delta^{13}C_{carb}$ data argue for a marine association with either: (1) the pre-Shuram anomaly (~600 Ma [10] to > 570-560 Ma (some time shortly following the ~580 Ma Gaskiers glaciation [5]); or (2) the post-Shuram anomaly (~551 to 542 Ma). However, extremely unradiogenic $^{87}Sr/^{86}Sr$ data well below Ediacaran values and the huge range of Ediacaran $\delta^{13}C_{carb}$ variation, which could support any number of apparent marine correlations, could also be consistent with (3) a non-marine/lacustrine setting, for which the age constraints retract to ≤600–530 Ma. More work in Jibalah Group carbonate basins is required to evaluate which of these depositional scenarios is most likely, and what is the associated significance for metazoan radiation.

ACKNOWLEDGMENTS

This evaluation is based on a 2005 reconnaissance survey made as part of other Cryogenian investigations in the Arabian shield. We thank the Saudi Geological Survey, especially Fayek Kataan, for field and logistics support, and warm hospitality during our 2005 investigations of the Arabian shield. Partial support from NSF grant EAR 0509486 is acknowledged. UT Dallas students assisted with fieldwork (Sumit Mukherjee and Kamal Ali) and sample analysis (Britney Blake). A modest grant from the UT Dallas School of Natural Science and Mathematics helped support geochemical analyses. We thank Alton Brown for helpful input regarding petrographic description and interpretation. Scott Carpenter supervised the analyses of stable isotopes (Iowa University). Comments and suggestions by W.G. Ernst and an anonymous reviewer helped to improve the manuscript.

REFERENCES

[1] P.F. Hoffman, A.J. Kaufman, G.P. Halverson, and D.P. Schrag, "A Neoproterozoic Snowball Earth", *Science,* **281**(1998), pp. 1342–1346.

[2] I. J. Fairchild and M. J. Kennedy, "Neoproterozoic Glaciation in the Earth System", *Journal of the Geological Society, London*, **164**(2007), pp. 895–921.

[3] R.J. Stern, D. Avigad, N.R. Miller, and M. Beyth, "From Volcanic Winter to Snowball Earth: An Alternative Explanation for Neoproterozoic Biosphere Stress", in *Links Between Geological Processes, Microbial Activities & Evolution of Life*, eds. Y. Dilek, H. Furnes, and K. Muehlenbachs. Approaches in Solid Earth Sciences (Springer), (in press).

[4] B.S. Kendall, R.A. Creaser, and D. Selby, "Re–Os Geochronology of Postglacial Black Shales in Australia: Constraints on the Timing of the 'Sturtian' Glaciation", *Geology*, **34**(2006), pp. 729–732.

[5] D.A Fike,. J.P. Grotzinger, L.M Pratt, and R.E. Summons, "Oxidation of the Ediacaran Ocean", *Nature*, **444**(2006), pp. 744–747.

[6] D.E. Canfield, S.W. Poulton, and G.M Narbonne, "Late-Neoproterozoic Deep-Ocean Oxygenation and the Rise of Animal Life", *Science*, **315**(2007), pp. 92–95.

[7] R.J. Stern, D. Avigad, N.R Miller, and M. Beyth, "Geological Society of Africa Presidential Review #10: Evidence for the Snowball Earth Hypothesis in the Arabian–Nubian Shield and the East African Orogen", *Journal of African Earth Sciences*, **44**(2006), pp. 1–20.

[8] K. A. Ali, R.J. Stern, W.I. Manton, P.R. Johnson, and S.K. Mukherjee, "The Neoproterozoic Atud Diamictite of the

Eastern Desert of Egypt and Northern Saudi Arabia: Evidence of Snowball Earth?", *Geological Society of America Bulletin*, (submitted).

[9] D. Avigad, A. Sandler, K. Kolodner, R.J. Stern, M.O. McWilliams, N. Miller, and M. Beyth, "Mass-Production of Cambrian Quartz-Rich Sandstone as a Consequence of Chemical Weathering of Pan-African Orogens: Implications for Global Environment", *Earth and Planetary Science Letters*, **240**(2005), pp. 818-826.

[10] E. Le Guerroué, P. Allen, A. Cozzi, J. Etienne, and M. Fanning, "50 Myr Recovery from the Largest Negative $\delta^{13}C$ Excursion in the Ediacaran Ocean", *Terra Nova*, **14**(2006), pp. 129–155.

[11] P. R. Johnson, "Post-Amalgamation Basins of the NE Arabian Shield and Implications for Neoproterozoic III Tectonism in the Northern East African Orogen", *Precambrian Research*, **123**(2003), pp. 321–337.

[12] P.R. Johnson and B. Woldehaimanot, "Development of the Arabian–Nubian Shield: Perspectives on Accretion and Deformation in the Northern East African Orogen and the Assembly of Gondwana", in *Proterozoic East Gondwana: Supercontinent Assembly and Break-up*, eds. M. Yoshida, B.F. Windley, and S. Dasgupta. Special Publication, Geological Society of London, **206**(2003), pp. 289–325.

[13] P.G. Nicholson and D. Janjou, "The Neoproterozoic Play in Saudi Arabia" (Abstract), *AAPG Annual Convention*, *Salt Lake City, Utah,* May 11-14, 2003.

[14] F.B. Davies, D.C. Frets, and M.R. Hanif, "The Reconnaissance Geology of the Wadi al Jizl Quadrangle, Sheet 36/37A, Kingdom of Saudi Arabia", *Saudi Arabian Deputy Ministry for Mineral Resources Open-File Report DGMR-OF-01-21*, **46** (1981), p. 6 figs., 1 pl.

[15] F. B. Davies, "Geologic Map of the Al Wajh Quadrangles, sheet 26B, Kingdom of Saudi Arabia", *Saudi Arabian Deputy Ministry for Mineral Resources Geoscience Map GM 83*, scale 1:250,000 (1985), 27 pp.

[16] J. Delfour, "Le Groupe de J'Balah, une nouvelle unite du Bouclier Arabe", *Bureau de Recherche Geologique et Minieres Bulletin,* (*Ser. 2*) **4**(**4**) (1970), pp. 19–32.

[17] D.G. Hadley, "The Taphrogeosynclinal Jubaylah Group in the Mashhad Area, Northwestern Hijaz, Kingdom of Saudi Arabia", *Saudi Arabian Directorate General of Mineral Resources Bulletin*, **10** (1974), 18 pp.

[18] P.A. Allen, "Snowball Earth and Neoproterozoic Basin Evolution on the Eastern Periphery of Gondwana: Implications for Petroleum Systems", in *Global Infracambrian Hydrocarbon Systems and the Emerging Potential in North Africa, Burlington House, London*, 29th–30th November 2006, 2006, pp. 6–8.

[19] C.E. Hedge, "Precambrian Geochronology of Part of Northwestern Saudi Arabia", *Saudi Arabian Deputy Ministry for Mineral Resources Open-File Report USGS-OF-04-31* (1984), 12 pp.

[20] A. Kennedy, P.R. Johnson, and F.H. Kattan, "SHRIMP Geochronology in the Northern Arabian Shield: Part III: Data Acquisition 2006", *Saudi Geological Survey Open-File Report* (in prep.).

[21] D. Avigad, K. Kolodner, M. McWilliams, H. Persing, and T. Weissbrod, "Origin of Northern Gondwana Cambrian Sandstone Revealed by Detrital Zircon SHRIMP Dating", *Geology*, **31**(2003), pp. 227–230.

[22] K. Kolodner, D. Avigad, M. McWilliams, and T.R. Ireland, "U–Pb SHRIMP Dating of Detrital Zircons from Paleozoic and Mesozoic Sandstone in Israel and Jordan", *Geophysical Research Abstracts*, **8**(2006), #00387.

[23] W. Compston, I.S. Williams, and C.E. Meyer, "U–Pb Geochronology of Zircons from Lunar Breccia 73217 Using a Sensitive High-Mass-Resolution Ion Microprobe", *Proceedings of the Fourteenth Lunar and Planetary Science Conference, Part 2. Journal of Geophysical Research*, **89B**(1984), pp. 525–534.

[24] I.S. Williams, "U–Th–Pb Geochronology by Ion Microprobe", in *Applications of Microanalytical Techniques to Understanding Mineralizing Processes*, ed. M.A. McKibben, W.C. Shanks, and W.I. Ridely, *Reviews in Economic Geology*, **7**(1998), pp. 1–35.

[25] R.H. Steiger and E. Jäger, "Subcommission on Geochronology: Convention on the Use of Decay Constants in Geo- and Cosmochronology", *Earth and Planetary Science Letters*, **36**(1977), pp. 359–362.

[26] M.J. Kennedy, N. Christie-Blick, and L.E. Sohl, "Are Proterozoic Cap Carbonates and Isotopic Excursions a Record of Gas Hydrate Destabilization Following Earth's Coldest Intervals?", *Geology*, **29**(2001), pp. 443–446.

[27] G.P. Halverson, P.F. Hoffman, D.P. Schrag, A.C. Maloof, and A.H.N. Rice, "Toward a Neoproterozoic Composite Carbon-Isotope Record", *Geological Society of America Bulletin*, **117**(2005), pp. 1181–1207.

[28] G.P. Halverson, F.Ö. Dudás, A.C. Maloof, and S.A. Bowring, "Evolution of the $^{87}Sr/^{86}Sr$ Composition of Neoproterozoic Seawater", *Palaeogeography, Palaeoclimatology, Palaeoecology,* **256**(2007), pp. 103–129.

[29] G. Shields and J. Veizer, "Precambrian Marine Carbonate Isotope Database: Version 1.1", *Geochemistry Geophysics Geosystems*, **3**(2002), pp. 1–12.

[30] J.B.D. Jaffrés, G.A. Shields, and K. Wallmann, "The Oxygen Isotope Evolution of Seawater: A Critical Review of a Long-Standing Controversy and an Improved Geological Water Cycle Model for the Past 3.4 Billion Years", *Earth-Science Reviews*, **83**(2007), pp. 83–122.

[31] J.L. Banner and G.N. Hanson, "Calculations of Simultaneous Isotopic and Trace Element Variations During Water–Rock Interaction with Applications to Carbonate Diagenesis", *Geochimica et Cosmochimica Acta*, **54**(1990), pp. 3123–3137.

[32] S.B. Jacobsen and A.J. Kaufman, "The Sr, C, and O Isotopic Evolution of Neoproterozoic Seawater", *Chemical Geology*, **161**(1999), pp. 37–57.

[33] T.M. Kusky and M.I. Matsah, "Neoproterozoic Dextral Faulting on the Najd Fault System, Saudi Arabia, Preceded Sinistral Faulting and Escape Tectonics Relative to Closure of the Mozambique Ocean", *Geological Society of London, Special Publications,* **206** (2003), pp. 327–361.

[34] R.E. Denison, R.B. Koepnick, A. Fletcher, M.W. Howell, and W.S. Calloway, "Criteria for the Retention of Original Seawater $^{87}Sr/^{86}Sr$ in Ancient Shelf Limestones", *Chemical Geology*, **112**(1994), pp. 131–143.

[35] G.D.Love, E. Grosjean, D.A. Fike, J.P. Grotzinger, S.A. Bowring, D. Condon, A.N. Lewis, C. Stalvies, C.E. Snape, and R.E. Summons, "A >90 Million Year Record of Neoproterozoic Sponges (Porifera) in the South Oman Salt Basin", *Proceedings of the 22nd International Meeting on Organic Geochemistry, Abstracts,* vol. 1, 2005, pp. 123–124.

[36] S.A. Wilde, and K. Youssef, "A Re-Evaluation of the Origin and Setting of the Late Precambrian Hammamat Group Based on SHRIMP U–Pb Dating of Detrital Zircons from Gebel Um Tawat, North-Eastern Desert", *Journal of the Geological Society, London*, **159**(2002), pp. 595–604.

[37] G.H. Jarrar, H. Wachendorf, and D. Zellmer, "The Saramuj Conglomerate: Evolution of a Pan-African Molasse Sequence from Southwest Jordan", *Neues Jahrbuch für Geologie und Paläontologie, Monatsheft*, **6**(1991), pp. 335–356.

[38] S. Bowring, P. Myrow, E. Landing, J. Ramezani, and J. Grotzinger, "Geochronological Constraints on Terminal Neoproterozoic Events and the Rise of Metazoans", *Geophysical Research Abstracts*, **5**(2003), p. 13,219.

[39] S.J. Burns, and A. Matter, "Carbon Isotopic Record of the Latest Proterozoic from Oman", *Eclogae Geologicae Helviticae*, **86**(1993), pp. 595–607.

[40] A. Cozzi, P.A. Allen, and J.P. Grotzinger, "Understanding Carbonate Ramp Dynamics Using $\delta^{13}C$ Profiles: Examples from the Neoproterozoic Buah Formation of Oman", *Terra Nova*, **16**(2004), pp. 62–67.

[41] S.A. Bowring, J.P. Grotzinger, D.J. Condon, J. Ramezani, and M. Newall, "Geochronologic Constraints on the Chronostratigraphic Framework of the Neoproterozoic Huqf Supergroup, Sultanate of Oman", *American Journal of Science,* **307**(2007), pp. 1097–1145.

[42] J.E. Amthor, J.P. Grotzinger, S. Schröder, S.A. Bowring, J. Ramezani, M.W. Martin, and A. Matter, "Extinction of *Cloudina* and *Namacalathus* at the Precambrian-Cambrian Boundary in Oman", *Geology*, **31**(2003), pp. 431–434.

[43] D. Condon, M. Y. Zhu, S. Bowring, W. Wang, A. H. Yang, and Y. G. Jin, "U–Pb Ages from the Neoproterozoic Doushantuo Formation, China", *Science*, **308**(2005), pp. 95-98.

[44] P.L. Knauth, "Temperature and Salinity History of the Precambrian Ocean: Implications for the Course of Microbial Evolution", *Palaeogeography, Palaeoclimatology, Palaeoecology*, **219**(2005), pp. 53–69.

[45] J.E. Amthor, J.P. Grotzinger, S. Schröder, and B.C. Schreiber, "Tectonically-Driven Evaporite–Carbonate Transitions in a Precambrian/Cambrian Saline Giant: Ara Salt Basin of South Oman", *American Association of Petroleum Geologists Annual Convention, March 10–13th, Houston, Abstract Volume,* 2002, p. A6-7.

[46] J.M. Hayes, H. Strauss, and A.J. Kaufman "The Abundance of ^{13}C in Marine Organic Matter and Isotopic Fractionation in the Global Biogeochemical Cycle of Carbon During the Past 800 Ma", *Chemical Geology*, **161**(1999), pp. 103–125.